NASA TN D-943

TECHNICAL NOTE

D-943

AERODYNAMIC CHARACTERISTICS, TEMPERATURE, AND NOISE MEASUREMENTS OF A LARGE-SCALE EXTERNAL-FLOW JET-AUGMENTED-FLAP MODEL WITH TURBOJET ENGINES OPERATING

By Marvin P. Fink

Langley Research Center
Langley Field, Va.

NATIONAL AERONAUTICS AND SPACE ADMINISTRATION
WASHINGTON

September 1961

NATIONAL AERONAUTICS AND SPACE ADMINISTRATION

TECHNICAL NOTE D-943

AERODYNAMIC CHARACTERISTICS, TEMPERATURE, AND NOISE MEASUREMENTS OF A LARGE-SCALE EXTERNAL-FLOW JET-AUGMENTED-FLAP MODEL WITH TURBOJET ENGINES OPERATING

By Marvin P. Fink

SUMMARY

An investigation has been conducted in the Langley full-scale tunnel on a large-scale model powered by turbojet engines with flattened rectangular nozzles. The wing had 35° sweep of the leading edge, an aspect ratio of 6.5, a taper ratio of 0.31, and NACA 65_1-412 and 65-408 airfoils at the root and tip. The investigation included measurements of the longitudinal aerodynamic characteristics of the model with half-span and full-span flaps and measurements of the sound pressure and skin temperature on the portions of the lower surface of the wing immersed in the jet flow. The tests were conducted over a range of angles of attack from -8° to 16° for Reynolds numbers from 1.8×10^6 to 4.4×10^6 and a range of momentum coefficients from 0 to 2.0.

In general, the aerodynamic results of this investigation made with a large-scale hot-jet model verified the results of previous investigations with small models powered by compressed-air jets. Although blowing was only done over the inboard portion of the wing, substantial amounts of induced lift were also obtained over the outboard portion of the wing. Skin temperatures were about 340° F and wing heating could be handled with available materials without cooling. Random acoustic loadings on the wing surface were high enough to indicate that fatigue failure from this source would require special consideration in the design of an external-flow jet flap system for an airplane.

INTRODUCTION

The increased low-speed performance requirements of highly loaded high-speed aircraft has led to the consideration of ways of utilizing the propulsion engines for lift augmentation during the landing and take-off phase of flight.

Boundary-layer control proved very effective in improving the performance characteristics of airplanes, but this method was limited by the small amount of air that could be drawn from the main power supply for application to boundary-layer control.

Another scheme was developed in which the entire mass flow of the engine could be utilized to augment the wing lift and attain much higher lift than could be reached by the low-mass-flow boundary-layer control systems. Two methods using the full-engine efflux were investigated. One was the internal system in which the jet was emitted from the trailing edge of the wing and directed downward by rotating the jet slot. The other was an external-flow arrangement such as might be used on an airplane with pod-mounted engines. In the latter method a flattened tailpipe or nozzle was attached to the engine to spread the engine exhaust into a thin jet sheet and to direct the sheet toward the slot of a trailing-edge flap. The jet sheet, passing through the flap slot, would be turned by the upper surface of the flap and, in addition to the direct thrust of the jet, would induce a flow over the wing ahead of the flap and thus cause a large increase in the circulation lift.

L 1 3 6 6

Previous research on the external-flow jet-augmented flap with small models (refs. 1 and 2) by using cold compressed-air jets to simulate engines showed such promising results that interest was prompted to investigate the principle with a large-scale model having turbojet engines as power sources. Some preliminary tests were made on a static test setup (ref. 3) to determine the feasibility of using a flattened tailpipe on a jet engine to spread the exhaust and to determine the static turning characteristics of a trailing-edge flap immersed in the jet sheet. The results of these tests were useful in the design of the large-scale model.

In addition to gaining large-scale aerodynamic data in the present investigation, it was also of interest to look into the environmental conditions to which the lower surface of the wing and flap would be subjected, specifically the temperature and acoustic pressure fluctuations to which the part of the wing immersed in the jet was subjected. Because of the specific nature and use of the temperature and noise data, however, these data will be presented herein without analysis.

The model used in the subject investigation was a low-wing—body configuration having the general wing geometric characteristics of current jet transports. The wing had an aspect ratio of 6.5, 35° sweepback of the leading edge, and a taper ratio of 0.31, and was tapered in thickness from 0.12c at the root chord to 0.08c at the tip. The power plants were YJ69-T-15 turbojet engines suspended in pod-type mounts from the leading edge.

Tests were conducted in the Langley full-scale tunnel for jet momentum coefficients from 0 to 2.0 and over an angle-of-attack range

from -8° to 16° at several flap deflections. Test Reynolds numbers varied from 1.8×10^6 to 4.4×10^6.

COEFFICIENTS AND SYMBOLS

C_L	lift coefficient, $\frac{\text{Lift}}{q_\infty S}$
C_D	drag coefficient, $\frac{\text{Drag}}{q_\infty S}$
C_m	pitching-moment coefficient about $0.25\bar{c}$, $\frac{\text{Pitching moment}}{q_\infty S\bar{c}}$
$C_{L,\Gamma}$	circulation lift coefficient
C_μ	momentum coefficient, $\frac{T}{q_\infty S}$
c	local wing chord measured parallel to plane of symmetry, ft
$\bar{c}$	mean aerodynamic chord, $\frac{2}{S}\int_0^{b/2} c^2 dy$, ft
b	wing span, ft
f	frequency, cps
S	wing area, sq ft
α	angle of attack, deg
q_∞	free-stream dynamic pressure, lb/sq ft
δ_f	flap deflection (relative to wing chord plane) measured perpendicular to flap hinge line, deg
η	jet turning and spreading efficiency factor, determined by ratio of thrust of jet reaction at flap to thrust at exhaust nozzle
θ	angle of resultant-force vector from horizontal
F_x	longitudinal component of jet reaction force

F_z vertical component of jet reaction force

W weight of airplane, lb

W_a engine inlet air flow, lb/sec

T or F_N engine gross thrust minus ram drag, $F_g - \frac{W_a}{g}$

g acceleration of gravity, 32.2 ft/sec^2

F_g gross static thrust, lb

MODEL

A sketch showing the model and some of its principal dimensions is given in figure 1. The model, which was a low-wing configuration, was tested without a horizontal tail. The wing had an aspect ratio of 6.5, a taper ratio of 0.31, and was sweptback 35° at the leading edge. The streamwise airfoil sections were NACA 65_1-412 and 65-408 at the root and tip, respectively. Figure 2 shows cross-sectional views of the flap geometry. Photographs of the model mounted in the full-scale tunnel test section are presented as figure 3.

A 0.25c trailing-edge flap extended from 0.11b/2 to the wing tip and was divided at the 0.55b/2 station so that half- and full-span flap configurations could be tested. Between the leading edge of the flap and the 65-percent-chord line was a section which could be deflected (see fig. 2) as a variable flap-slot entrance ramp. The flap was attached to the wing with brackets which provided a range of flap deflections as well as vertical and fore-and-aft positioning of the flap. On the model the ramp and flap were operated independently but on an airplane it would be presumed that both would be deflected together to form the proper ramp angle and slot height.

The YJ69-T-15 turbojet engines on this model were mounted on pylons extending from the wing leading edge at the 0.31b/2 station. The engines were hung in yokes so that the thrust axis of the engine could be rotated from a position parallel to the wing chord to a position that would aline the thrust axis with the flap slot. The tilt angle with the engines in the up position was about 8°. The engines were fitted with modified tailpipes (fig. 3) to provide a flattened jet sheet. The flattened nozzles selected for these tests were based on the results of some preliminary static tests reported in reference 3 and were constructed by joining six individual tubes to form a transition from a circular to a rectangular cross section at the exit.

In order to conduct heat away from the model during extended tunnel test periods, water-cooled Inconel panels were installed on the lower surface where the jet impinged on the skin. Note the darker unpainted surface in figure 3. As determined from the static tests of reference 3, the steel flap did not need heat protection; later results showed that the wing cooling was not absolutely necessary.

For the skin temperature and dynamic sound-pressure measurements, the right inboard water-cooled panel was replaced by one made of type 347 stainless steel with thermocouples installed according to the diagram in figure 4(a). The sound measurements were taken with microphones at the locations indicated by figure 4(b). The thermocouples were arranged in a pattern to cover an area on the lower surface of the wing where the engine exhaust would impinge. Shielded thermocouples were also installed in the same location and at a distance of about 1 inch from the skin in an effort to determine the exhaust-gas temperature. The noncooled panel was backed with 2 inches of insulation.

TESTS AND CORRECTIONS

Tests

Some preliminary tests were made with the half-span flap deflected 60° at $\alpha = 0^\circ$ over a range of C_μ to determine the effect of flap position on lift. In these tests, for a given slot gap, the flap was moved fore and aft to re-position the slot minimum with respect to the trailing edge of the ramp. A range of slot gaps from about 1.0 to 5.0 percent of the wing chord was tested. From these tests on the 60° deflected flap, it was found that the flap was most effective with a slot height-chord ratio of about 0.03 and with the flap positioned to form the slot minimum just ahead of the maximum thickness of the flap. On the basis of this result, the remainder of the force tests were made with the flap position and gap illustrated in figure 2.

The force data, taken on the tunnel six-component scale-balance system, were measured over the angle-of-attack range from -8° to 16° for a range of Reynolds number from 1.8×10^6 to 4.4×10^6. The angle-of-attack range was covered for power-on conditions of $C_\mu = 0$ to 1.5 with the engines level and with the engines tilted for the flap-up condition and for $C_\mu = 0$ to 2.0 for the flap-down configuration. The flap-down tests were made for flap deflections of 30°, 40°, and 60° for both half-span and full-span configurations.

The sound-pressure measurements were taken for the 60°-deflection half-span flap configuration at angles of attack of -8°, 0°, and 8° for

values of C_μ of 0.32, 0.67, 0.94, and 2.00 for six locations on the wing and four locations along the trailing edge of the flap. Only two microphones were used in the tests and they had to be moved to the various locations to get the area coverage. The output from the microphones was fed into a tape recorder. These tapes were run through an analyzer to obtain the mean-square differential pressures. Wing surface temperatures were taken simultaneously with the noise data for 12 thermocouple locations covering the area on the bottom of the wing shown in figure 4.

Corrections

The data have been corrected for airstream misalinement, buoyancy, and jet boundary effects. The momentum coefficient C_μ presented in this report was determined from static calibrations of the gross thrust of the engine rather than calculated mass flow at the nozzle. Total pressure in the tailpipe calibrated against static thrust of the engine was used as a basis for establishing power-on test conditions. The final thrust value used in determining C_μ as presented includes the ram drag which was determined from rakes mounted in the engine inlet.

RESULTS AND DISCUSSION

Power-Off Aerodynamic Characteristics

Because the power-on tests were to be made for a range of C_μ which would be varied by holding the thrust constant and changing the wind velocity, it was necessary to know whether a Reynolds number effect on the model was being introduced into the test results. The basic model was tested over a range of Reynolds numbers from 1.8×10^6 to 4.4×10^6 for tunnel dynamic pressures equivalent to those for the power-on tests and these results are shown in figure 5. As indicated by the increase in lift and negative pitching moment and the decrease in drag at the high angles of attack, separation on the outboard wing sections was delayed by increasing Reynolds number. In the angle-of-attack range where most of the test data were taken, however, Reynolds number effect was small.

A comparison of the longitudinal aerodynamic characteristics of the half-span and full-span flap deflection configuration is shown in figure 6 for flap deflections of 30°, 40°, and 60° with power off. The 40° deflection was the most effective, in terms of maximum lift produced, since, without boundary-layer control, this angle was about the highest for which an unseparated flow could be obtained. The lower lift-curve

slope for $\delta_f = 60^\circ$ is indicative of separated flow on the flap. The aerodynamic characteristics for the full-span and half-span flap configurations were qualitatively about the same, the differences in incremental lift due to the flap being about as would be expected. There was an appreciable increase in lift caused by deflecting the full-span flap, but, as has been shown before with swept wings, the increment in pitching moment is also appreciably increased. In these tests increasing the flap span from 0.44b/2 to 0.89b/2 almost doubled the pitching-moment coefficient (fig. 6), whereas little change occurred in the stability of the model.

Power Effects With Flaps Neutral

The results of power-on tests with the flaps retracted are presented in figures 7 and 8. The data of figure 7 are for the normal flight condition with the thrust axis parallel to the chord line (see fig. 1) and the data of figure 8 are for the 0° deflection jet-augmented-flap condition with the engine tilted 8°.

Since the angle of tilt of the thrust axis was small, and since the wing probably turned the jet exhaust in a chordwise direction, the effect of the engine tilt on drag was small. When the engines were tilted, however, there was a slight reduction in net thrust (negative drag) which might be partly attributed to the drag of the jet exhaust on the lower surface of the wing.

There was a decided increase in lift-curve slope with increasing C_μ with the engines either level or tilted. Part of the increase in lift-curve slope can be attributed directly to the contribution of engine thrust, but there was also a larger increase in lift on the wing induced by the engine exhaust flow. The data also show that there was a net gain in lift coefficient with increased C_μ at angles of attack above about 4° with the engines tilted 8° (fig. 8), but that for normal-flight configuration with the engines level there was a considerable loss in lift at low angles of attack. This loss in lift was probably caused by a negative pressure on the underside of the wing induced by the adjacent jet flow.

Tilting the engine brought the thrust axis much closer to the moment center of the model and consequently reduced the large positive pitching moments. There was also a slight improvement in the longitudinal stability when the engines were tilted.

Static Turning Efficiency

The length of the inboard flap was chosen so that the flap would just span the width of the jet sheet at the trailing edge of the wing for the static, that is, zero airspeed condition. Static tests with the partial-span flap deflected indicated that the turning efficiency for this configuration was about equal to that for the full-span flap (fig. 9). This result would be expected since very little of the outboard segment of the flap was immersed in the jet sheet. Turning efficiency η for the 30° and 40° flap deflection with values of efficiency of 0.87 and 0.82, respectively, was slightly higher than that for the 60° flap. The jet turning angle for $\delta_f = 30°$ was higher than the flap-deflection angle, whereas for $\delta_f = 40°$ and 60° the turning angle was slightly less. Even for the 30° flap deflection, the turning angle was less than the deflection angle of the upper surface of the flap. (See fig. 2.)

L
1
3
6
6

Jet Augmentation With Flaps Deflected

The basic data of figures 10 and 11 for half-span and full-span flap configurations with flaps deflected 30°, 40°, and 60° show, in general, an increase in lift coefficient and an increase in lift-curve slope with increasing C_μ. The data for $\alpha = 0°$ are replotted against C_μ in figure 12, and the additional circulation lift component $C_{L,\Gamma}$ was obtained from these plots and presented in figure 13. The data of figure 13 show the increase in $C_{L,\Gamma}$ with flap deflection for the partial-span flap configuration. The data also show that the circulation lift is increased considerably by deflecting the outboard flap segment and that the increase is greater for the higher flap deflections. The divergence of the $C_{L,\Gamma}$ curves for the half-span and full-span flaps indicates that lift was induced on the outer portion of the wing by jet flowing even though practically none of the outboard flap was immersed in the jet sheet. The pressure-distribution data of references 4 and 5 for a high-lift flap show that the amount of lift induced outboard was a function of the loading on the inboard portion of the wing.

The lift data from figures 12(c) and 13 for the full-span flap with 60° deflection are compared in figure 14 with similar data from reference 2 obtained on small-scale models with single-slotted and double-slotted flaps. The circulation lift for the large-scale model of the present investigation was greater than that obtained with the two small-scale models. Some of this difference, however, can be attributed to the fact that the flap on the large-scale wing was partially stalled with no blowing, as pointed out earlier in the discussion of figure 6.

The lift gained when this stalling was cleared up by blowing shows up in figure 14 as additional circulation lift. A similar effect was probably obtained with the small-scale single-slotted-flap model but not with the double-slotted-flap model.

The lift data are summarized in figure 15. This figure shows a plot of the variation of C_L at $C_D = 0$ with C_μ for half-span and full-span flap deflections ranging from 30° to 60°. It must be noted that the curve represents an untrimmed pitch condition, and no adjustments have been applied to account for the drag caused by a horizontal tail deflected for longitudinal trim. The dashed lines represent thrust-weight ratios of 0.1, 0.2, 0.3, and 0.4. The solid curve would, in a sense, represent a flight boundary. To the left of the curve the airplane would not have power required for steady level flight. To the right of the solid curve the airplane would, at the indicated thrust-weight ratio have an excess thrust available for an acceleration or climb condition.

Current subsonic jet transports are operating with ratios of thrust to take-off gross weight ranging from about 0.2 to 0.3. Figure 15 shows that for these thrust-weight ratios the maximum lift coefficients attainable at take-off would range from 1.65 to 2.35 with the half-span flap and from 2.3 to 3.5 with the full-span flap. These values would have to be reduced somewhat to allow for a sufficient margin of thrust for acceleration and climb.

The landing thrust-weight ratios (based on maximum allowable landing weight) of these same transports range from about 0.3 to 0.4. As can be seen in figure 15, the maximum lift coefficients ranged from 2.40 to 3.35 with the half-span flap, and from 3.6 to 4.8 with the full-span flap.

It may be noted that the large increase in lift coefficient (from $C_L = 1.25$ to 4.8 for the full-span flap) gained with augmentation would be reflected directly in an appreciable decrease in landing speed. With a wing loading of 70 pounds per square foot the landing speed of an airplane using this system could possibly be reduced from about 128 knots to 66 knots.

Temperature Measurements

Temperature measurements taken from thermocouples welded to the skin at the 12 different locations shown in figure 4 are presented in tables I and II. The maximum skin temperature (about 340° F) and the maximum gas temperature (about 460° F) were well below the maximum tailpipe temperature values of about 900° F and are low enough so that

very little insulation would be required to protect the structure. The reason for the low temperatures of the jet exhaust near the surface of the wing is believed to be the rapid mixing of the entrained air with the thin jet sheet. Literature published by the engine manufacturer shows that, at a distance of 6 tailpipe diameters (54 inches) behind the round nozzle, the maximum wake temperature was still about 500° F. With a flat nozzle as used in this investigation having an exit height of 1.5 inches (comparable to the diameter of a round jet), it might be reasoned then that the jet would be well mixed and cooled by the entrained air at a distance of 10 nozzle heights behind the exit. Temperature measurements at stations 6, 7, and 8 which are about 15 inches behind the nozzle show skin temperatures on the order of 23 percent to 30 percent of the tailpipe temperature.

L
1
3
6
6

Sound Pressures

Instances have been noted where structural members in aircraft have developed fatigue failures from the oscillatory loads imposed by pressure fluctuations from jet engines. These failures, in general, have been in secondary members such as nonstructural sections of the aircraft skin. For aircraft with pod-mounted engines, the trailing-edge flap and undersurfaces of the wings are particularly susceptible to such noise damage. This problem has been partially alleviated on some airplanes by locating the engine as far rearward as possible. Aircraft employing the external-flow jet-augmented flap would naturally be limited as to possible engine location since the nozzle would have to be some distance ahead of the flap slot.

The results of tests made with cold and hot jets (ref. 6) indicate that the presence of a reflection plane parallel with the thrust axis causes an increase in the amplitude of the fluctuating sound pressures at the surface over those at the same distance from a free jet.

Since on a jet-augmented-flap airplane a large portion of the undersurface of the wing is actually immersed in the jet flow, it was of interest to take some measurements of the fluctuating sound pressures in the region affected. Measurements were taken with a microphone mounted flush with the surface in the positions indicated in figure 4. The data of figure 16 were taken at angles of attack of -8.0°, -0.9°, and 6.4° over a range of C_μ with the half-span flap deflected 60° and are presented in the form of power-spectral-density analyses.

No consistent trends are indicated for all the test stations except that the maximum mean-square differential pressure (pounds per square inch per cycle per second) occurred in the lower frequency range.

An indication of the overall noise level is given by the area under the spectral density curves. Although the overall noise level is not the predominant factor in determining fatigue failures, it does give relative values of noise input. The curves for position E were integrated and sound pressures from 2.86 pounds per square foot to 22.46 pounds per square foot were observed. A maximum sound pressure of 25.94 pounds per square foot which converts to an overall loading value of 151 decibels was noted, however, at position C for a C_μ of 0.67 at $\alpha = 6.4^\circ$.

Investigations, with test samples, made to determine the effect of acoustic loadings on structural failure (refs. 7 and 8) indicate that, for the type of random spectra generated by turbojet and rocket engines, fatigue damage can occur at overall levels of the order of 140 decibels or higher. Incurred damage, of course, is dependent on the detail design of the structure, length of exposure, and the spectrum of the noise. From this investigation it appears that the sound-pressure levels for an external-flow, jet-augmented-flap application would be high enough to warrant special analysis of the individual case.

CONCLUSIONS

The results of wind-tunnel tests on a large-scale external-flow jet-augmented-flap model to determine the aerodynamic forces, wing surface temperatures, and random acoustic loadings yielded the following conclusions:

1. In general, the results of this investigation made with a large-scale hot-jet model verified the results of previous investigations with small models powered by compressed-air jets.

2. Although blowing was only done over the inboard portion of the wing, substantial amounts of induced lift were also obtained over the outboard portion of the wing.

3. Wing surface temperatures measured in the jet stream indicate that wing heating would not be an insurmountable problem with use of present-day materials and insulation. The maximum measured skin temperature was 340° F.

4. Measurements of the random acoustic loads on the wing lower surface show total loading values (151 decibels) high enough to warrant special consideration in structural design.

Langley Research Center,
National Aeronautics and Space Administration,
Langley Field, Va., June 21, 1961.

REFERENCES

1. Campbell, John P., and Johnson, Joseph L., Jr.: Wind-Tunnel Investigation of an External-Flow Jet-Augmented Slotted Flap Suitable for Application to Airplanes With Pod-Mounted Jet Engines. NACA TN 3898, 1956.

2. Johnson, Joseph L., Jr.: Wind-Tunnel Investigation of a Small-Scale Sweptback-Wing Jet-Transport Model Equipped With an External-Flow Jet-Augmented Double Slotted Flap. NASA MEMO 3-8-59L, 1959.

3. Fink, Marvin P.: Static Tests of an External-Flow Jet-Augmented Flap Test Bed With a Turbojet Engine. NASA TN D-124, 1959.

4. McLemore, H. Clyde, and Fink, Marvin P.: Surface Pressure Distributions on a Large-Scale 49° Sweptback Wing-Body-Tail Configuration With Blowing Applied Over the Flaps and Wing Leading Edge. NACA RM L57K25, 1958.

5. Whittle, Edward F., Jr., and McLemore, H. Clyde: Aerodynamic Characteristics and Pressure Distributions of a 6-Percent-Thick 49° Sweptback Wing With Blowing Over Half-Span and Full-Span Flaps. NACA RM L55F02, 1955.

6. Lassiter, Leslie W., and Hubbard, Harvey H.: The Near Noise Field of Static Jets and Some Model Studies of Devices for Noise Reduction. NACA Rep. 1261, 1956. (Supersedes NACA TN 3187.)

7. Hess, Robert W., Herr, Robert W., and Mayes, William H.: A Study of the Acoustic Fatigue Characteristics of Some Flat and Curved Aluminum Panels Exposed to Random and Discrete Noise. NASA TN D-1, 1959.

8. Hess, Robert W., Fralich, Robert W., and Hubbard, Harvey H.: Studies of Structural Failure Due to Acoustic Loading. NACA TN 4050, 1957.

TABLE I.- SKIN-TEMPERATURE MEASUREMENTS

Thermocouple position	Skin-temperature measurements, °F, for -														
	C_μ = 0.32 at -			C_μ = 0.67 at -			C_μ = 0.94 at -			C_μ = 2.00 at -			Static thrust at -		
	α, deg, of -			α, deg, of -			α, deg, of -			α, deg, of -			α, deg, of -		
	-8.0	-0.9	6.2	-8.0	-0.9	6.2	-8.0	-0.9	6.2	-8.0	-0.9	6.2	-8.0	-0.9	6.2
1	225	225	230	230	215	215	215	215	210	240	235	245	155	155	150
2	220	215	215	210	200	205	205	200	205	225	230	240	215	200	140
3	220	210	215	225	205	205	220	225	205	230	230	245	240	210	155
4	215	205	210	205	205	205	195	150	200	205	220	230	210	190	140
5	225	220	230	225	225	230	210	220	225	220	225	240	290	215	150
6	230	240	245	225	230	250	230	205	235	230	235	240	300	245	205
7	230	245	250	225	240	260	245	230	250	240	240	245	340	325	240
8	230	245	230	220	220	255	235	225	255	240	245	250	310	275	240
9	200	245	235	220	230	250	220	215	250	235	240	250	240	240	210
10	210	230	215	160	220	200	190	150	205	235	235	240	215	230	200
11	230	240	235	230	220	230	230	225	230	235	240	240	325	250	225
12	215	225	230	205	220	210	190	205	215	240	240	245	160	165	150
Tailpipe temperature	880	880	885	905	905	905	910	910	910	890	895	920			

TABLE II.- AIR-TEMPERATURE MEASUREMENTS

Thermocouple position	Air-temperature measurements, °F, for -														
	C_μ = 0.32 at -			C_μ = 0.67 at -			C_μ = 0.94 at -			C_μ = 2.00 at -			Static thrust at -		
	α, deg, of -			α, deg, of -			α, deg, of -			α, deg, of -			α, deg, of -		
	-8.0	-0.9	6.2	-8.0	-0.9	6.2	-8.0	-0.9	6.2	-8.0	-0.9	6.2	-8.0	-0.9	6.2
1	270	320	460	310	365	450	325	380	455	370	415	315	350	320	330
2	270	325	460	310	365	450	325	385	455	375	415	325	350	305	320
3	270	325	460	310	365	450	325	385	455	395	415	330	335	305	330
4	270	325	460	310	365	450	325	375	455	390	400	330	330	325	350
5	270	325	460	310	365	450	325	370	455	360	375	330	345	320	320
6	270	325	460	310	365	450	325	370	455	360	380	335	350	320	335
7	270	325	460	310	365	450	325	385	455	370	400	325	350	300	320
8	270	325	460	310	365	450	325	365	455	355	400	325	345	300	340
9	270		460	310	365	450	325	375	455	355	405	325	340	305	325
10	270		460	310	365	450	325	380	455	355	410	320	350	330	325
11	270		460	310	365	450	325	375	455	400	410	330	340	325	325
12	270		460	310	365	450	325	380	455	370	415	340	350	325	325

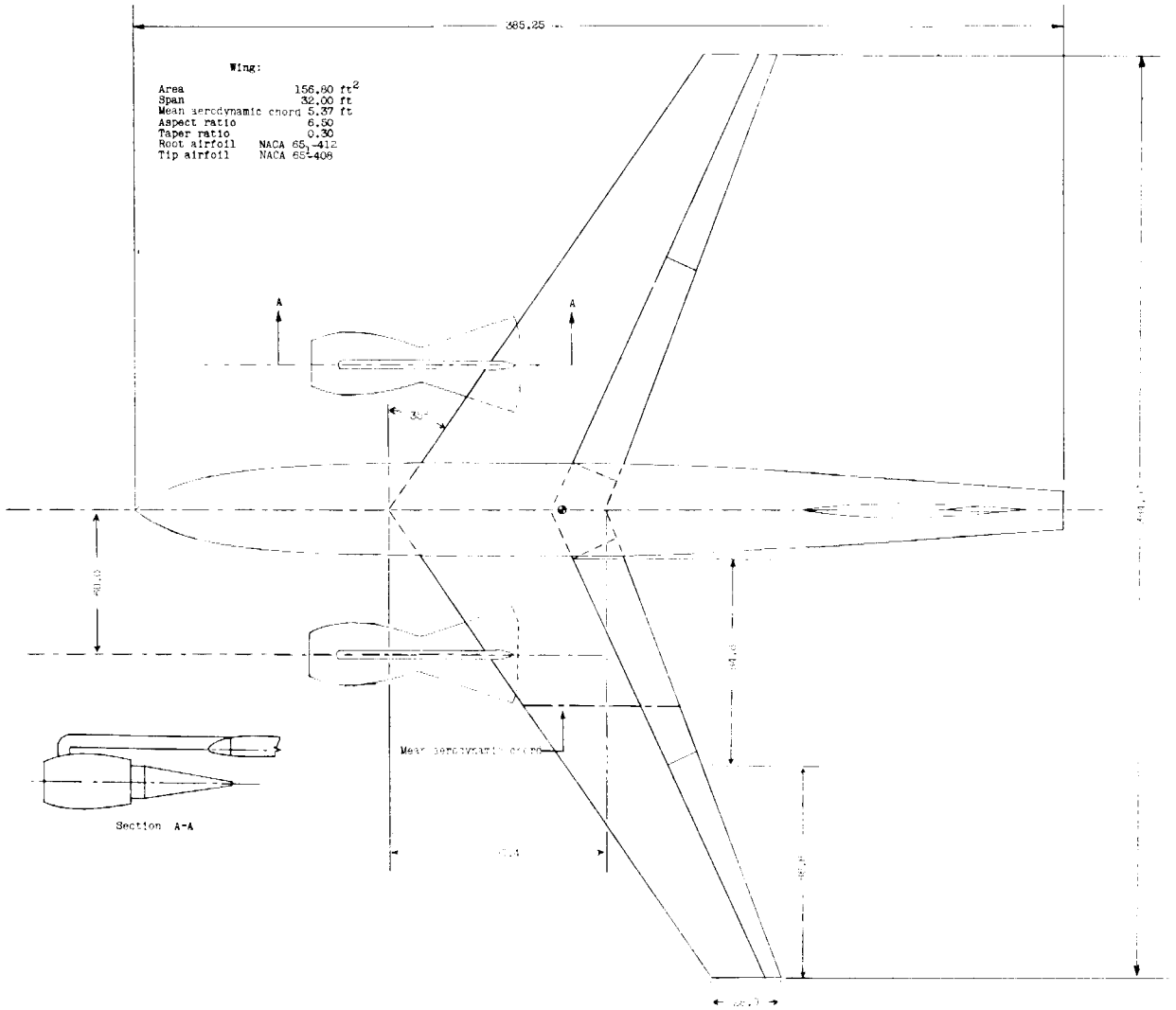

Figure 1.- Principal dimensions of the model. All measurements are in inches.

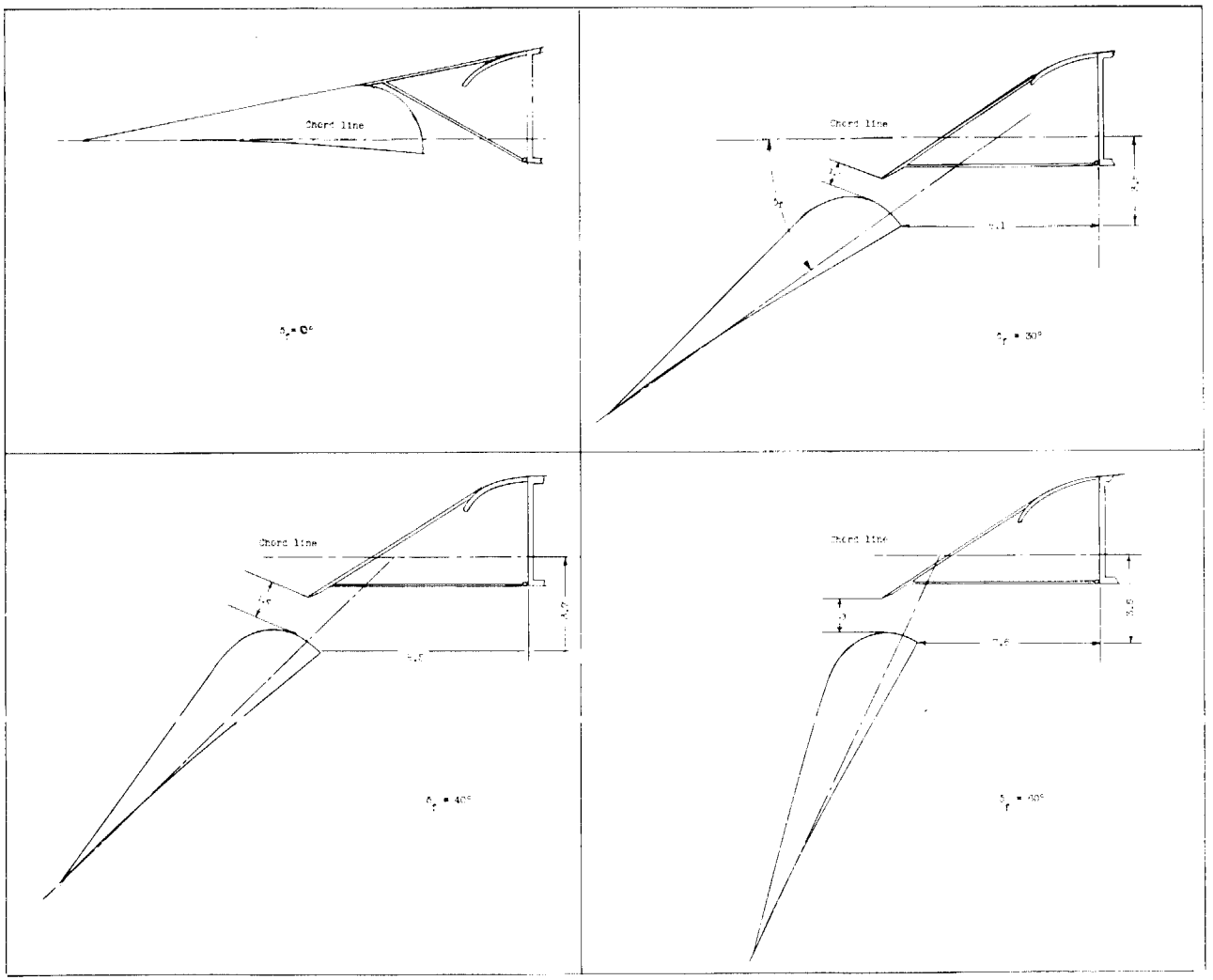

Figure 2.- Cross-sectional views of basic wing and with flaps deflected. Sections shown are normal to the 65-percent spar and at the juncture between the inboard and outboard flap. All dimensions are in inches.

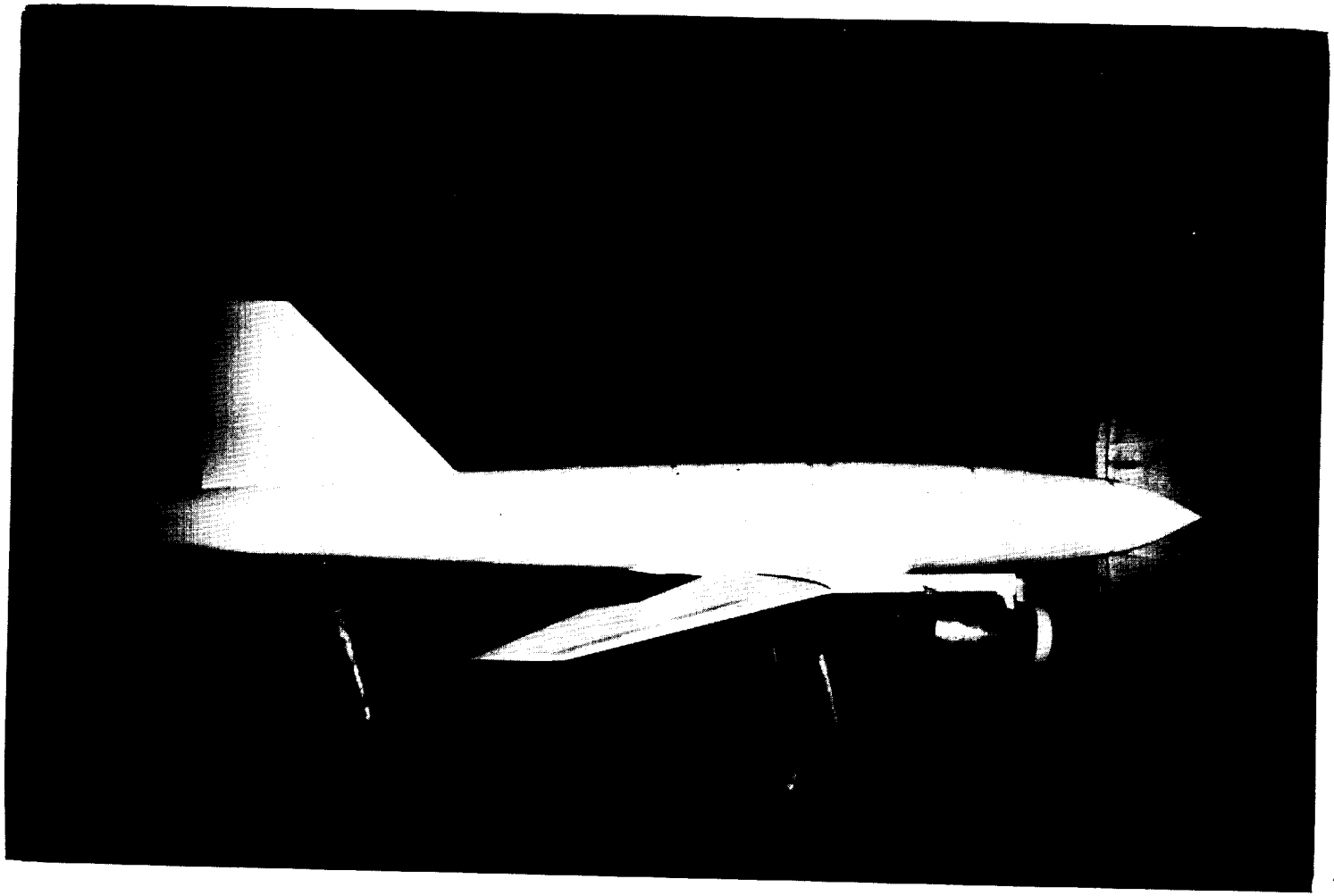

(a) Side view.

L-59-6923

Figure 3.- Photographs of the model in the tunnel.

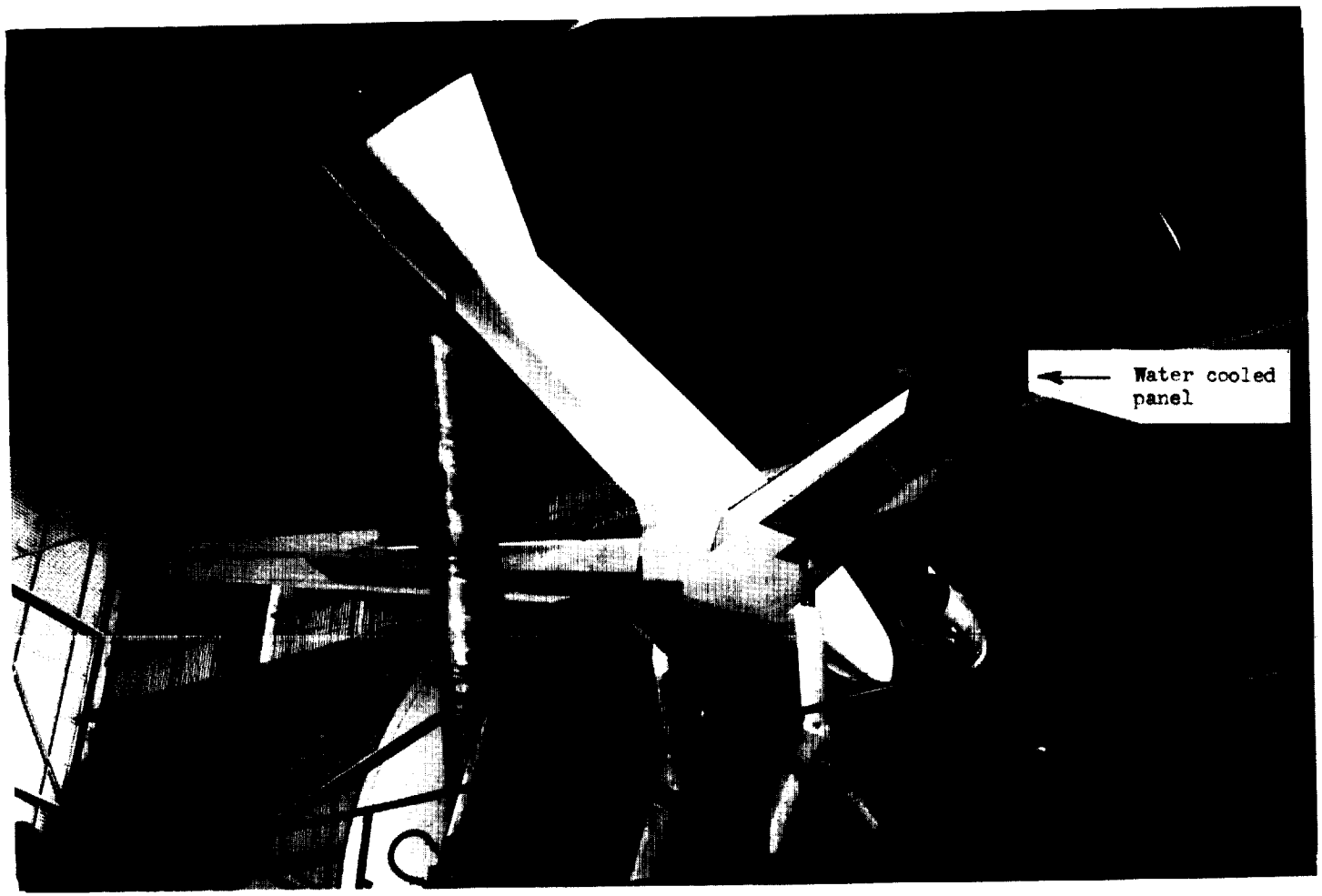

(b) View of model showing heat protective panels and flared nozzles. L-59-6924.1

Figure 3.- Concluded.

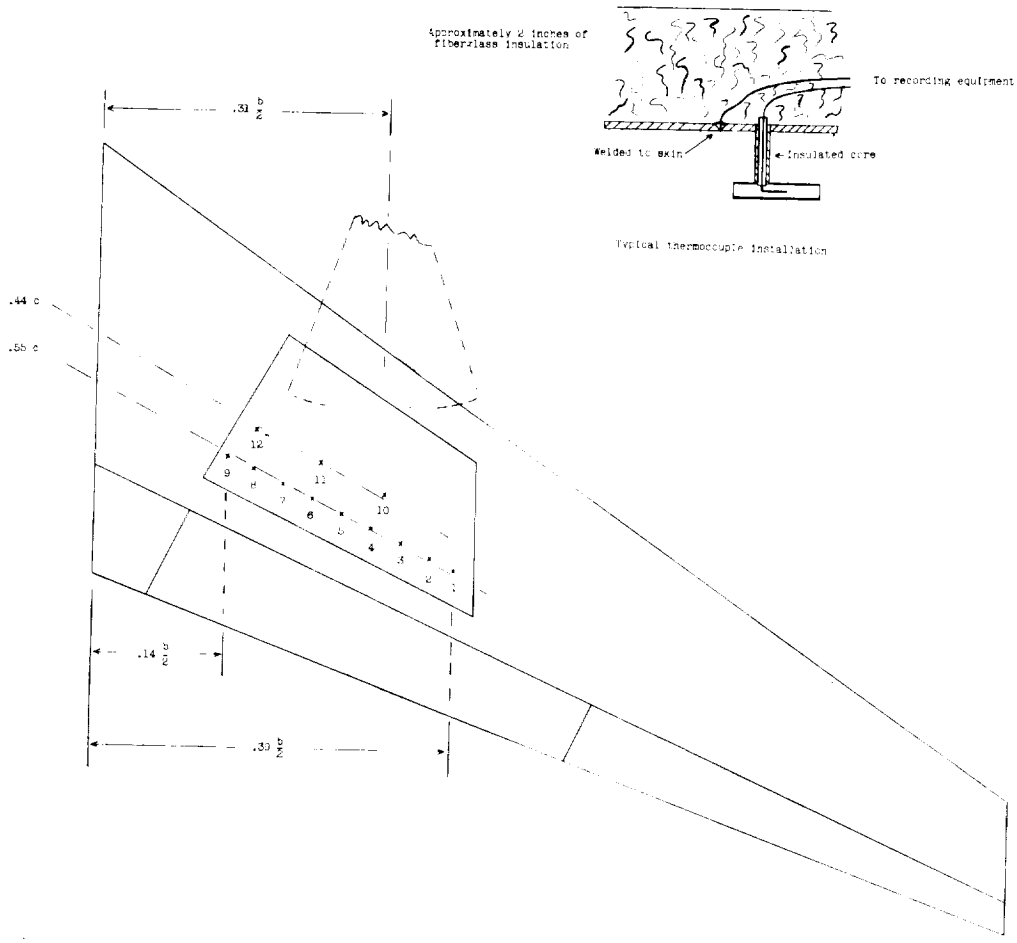

(a) Locations of thermocouples for skin-temperature measurements.

Figure 4.- Location of sound and temperature measuring stations.

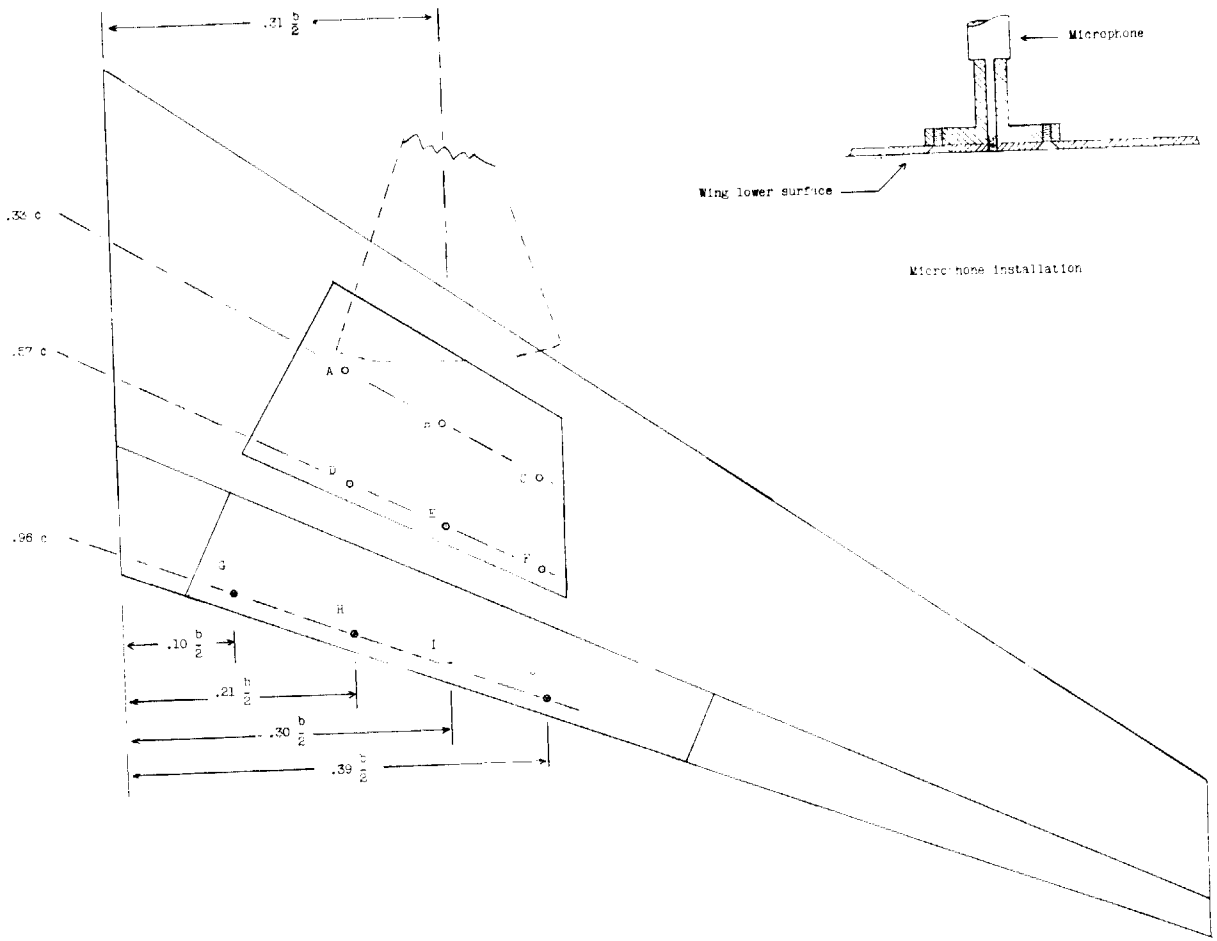

(b) Locations of the microphone for sound-pressure measurements.

Figure 4.- Concluded.

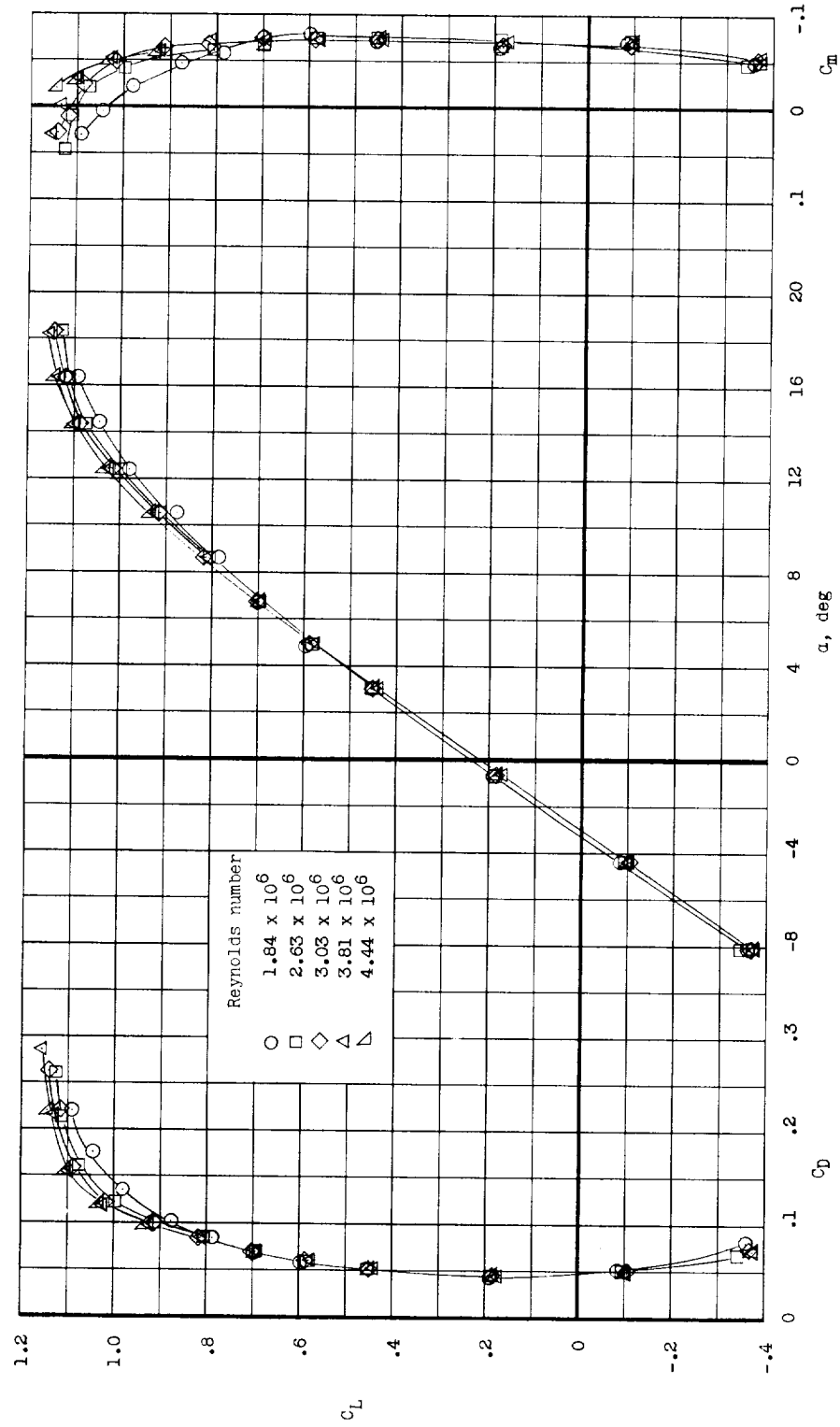

Figure 5.- Effect of Reynolds number on the aerodynamic characteristics of the basic model. $\delta_f = 0^\circ$; $C_\mu = 0$.

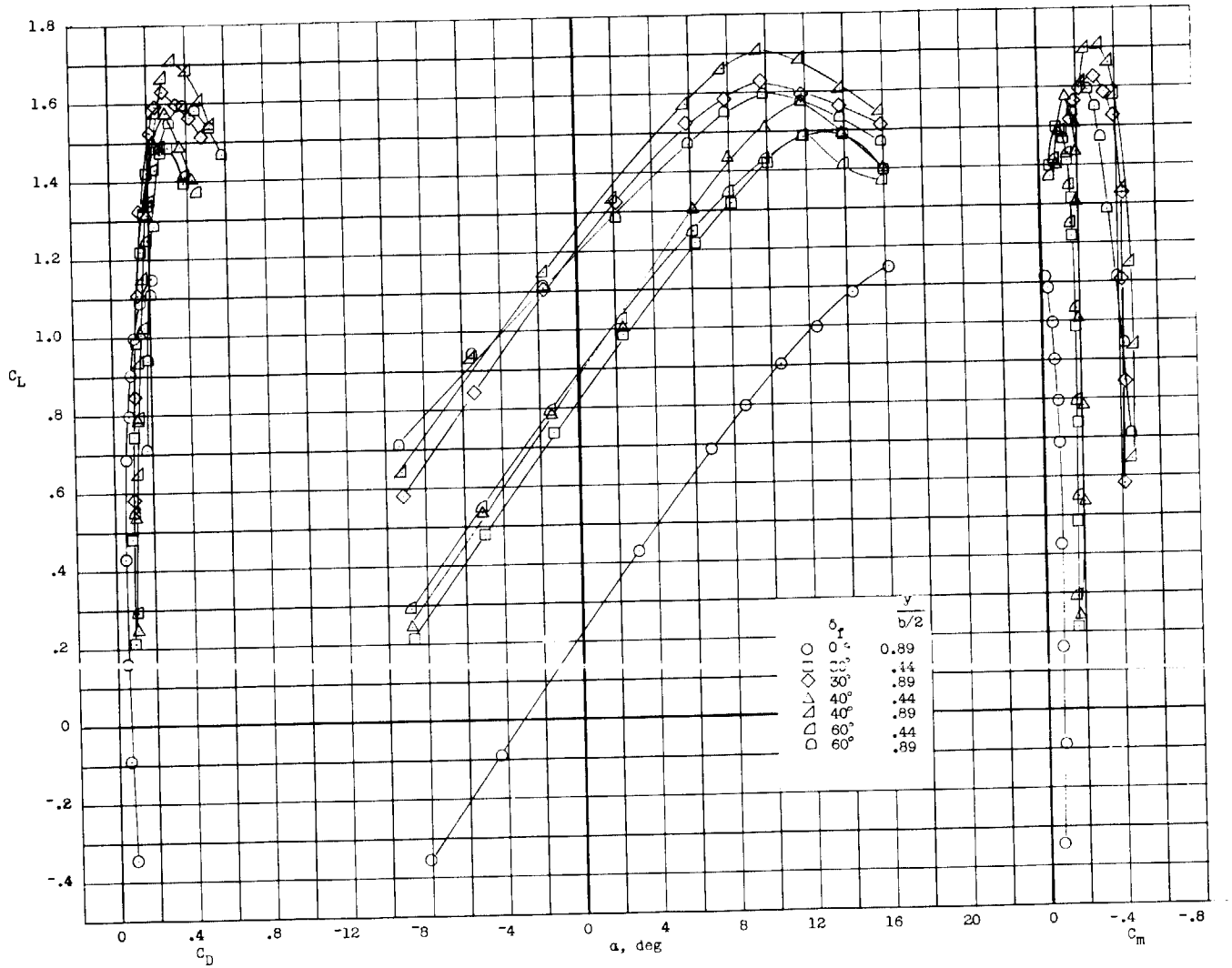

Figure 6.- Aerodynamic characteristics of the model for several flap deflections. Half- and full-span configuration. $C_\mu = 0$.

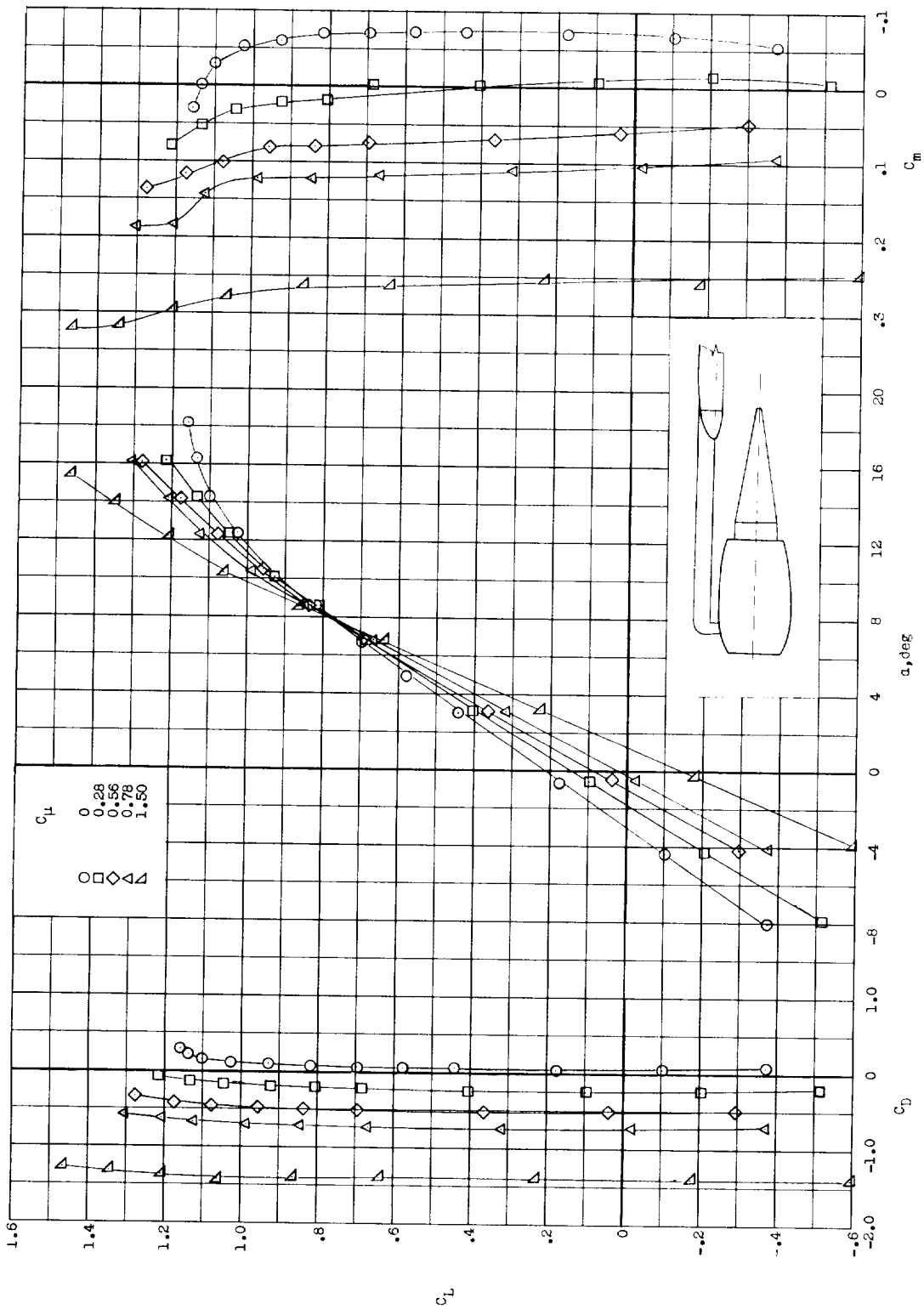

Figure 7.- Effect of thrust coefficient on the aerodynamic characteristics of the model in the cruise configuration. $\delta_f = 0^o$.

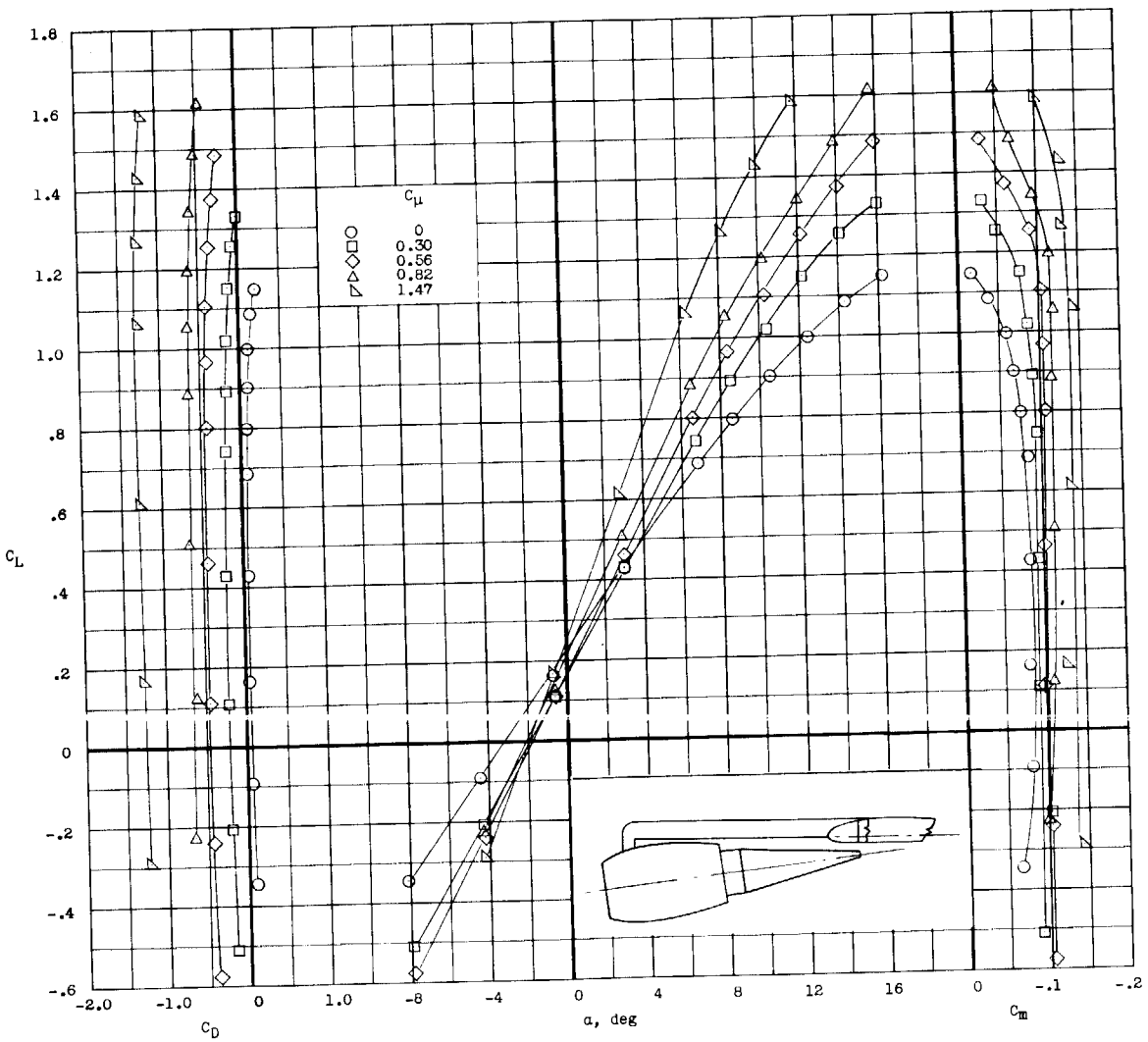

Figure 8.- Aerodynamic characteristics of the basic model configuration with the engines tilted. $\delta_f = 0^o$.

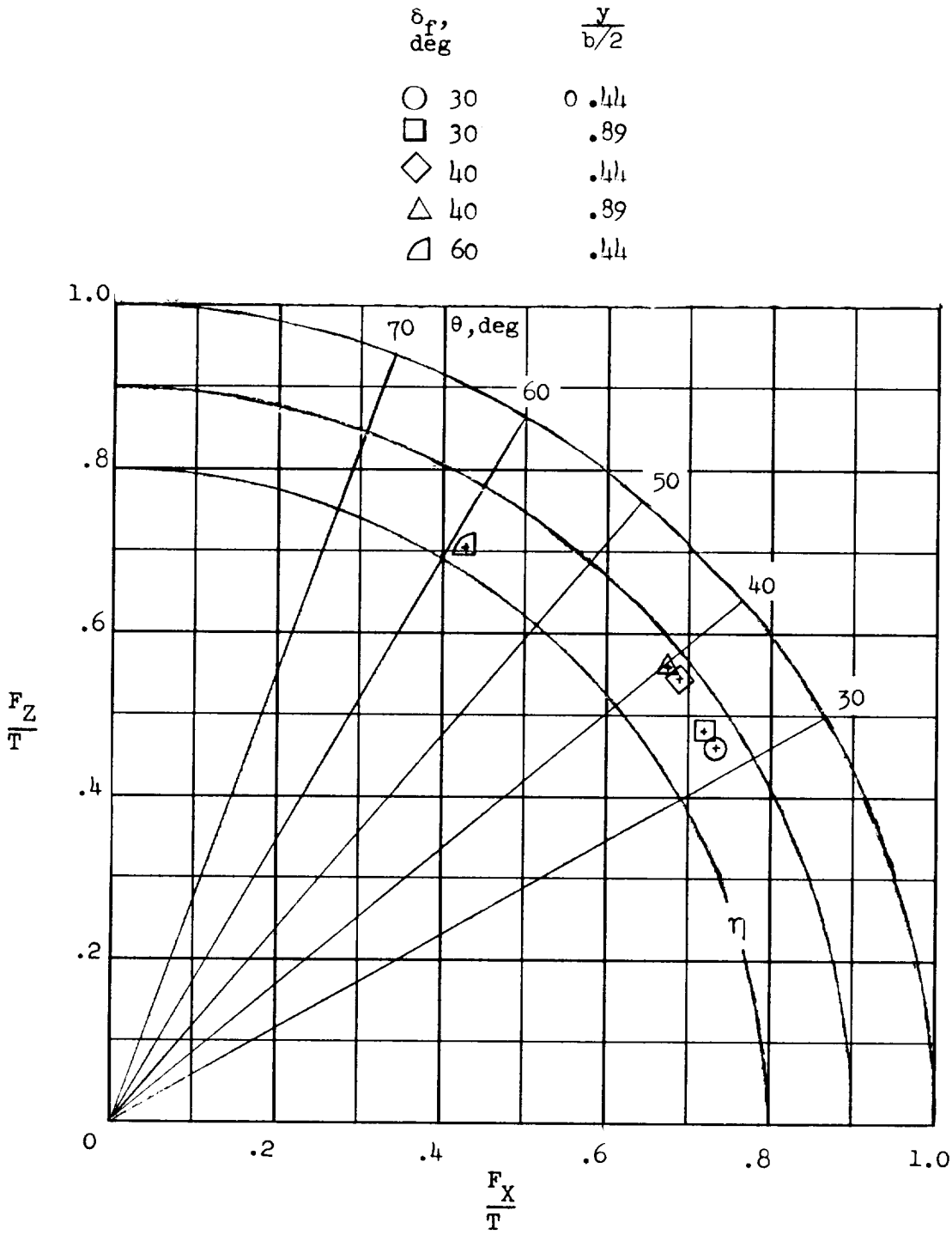

Figure 9.- Summary of turning efficiency and turning angle.

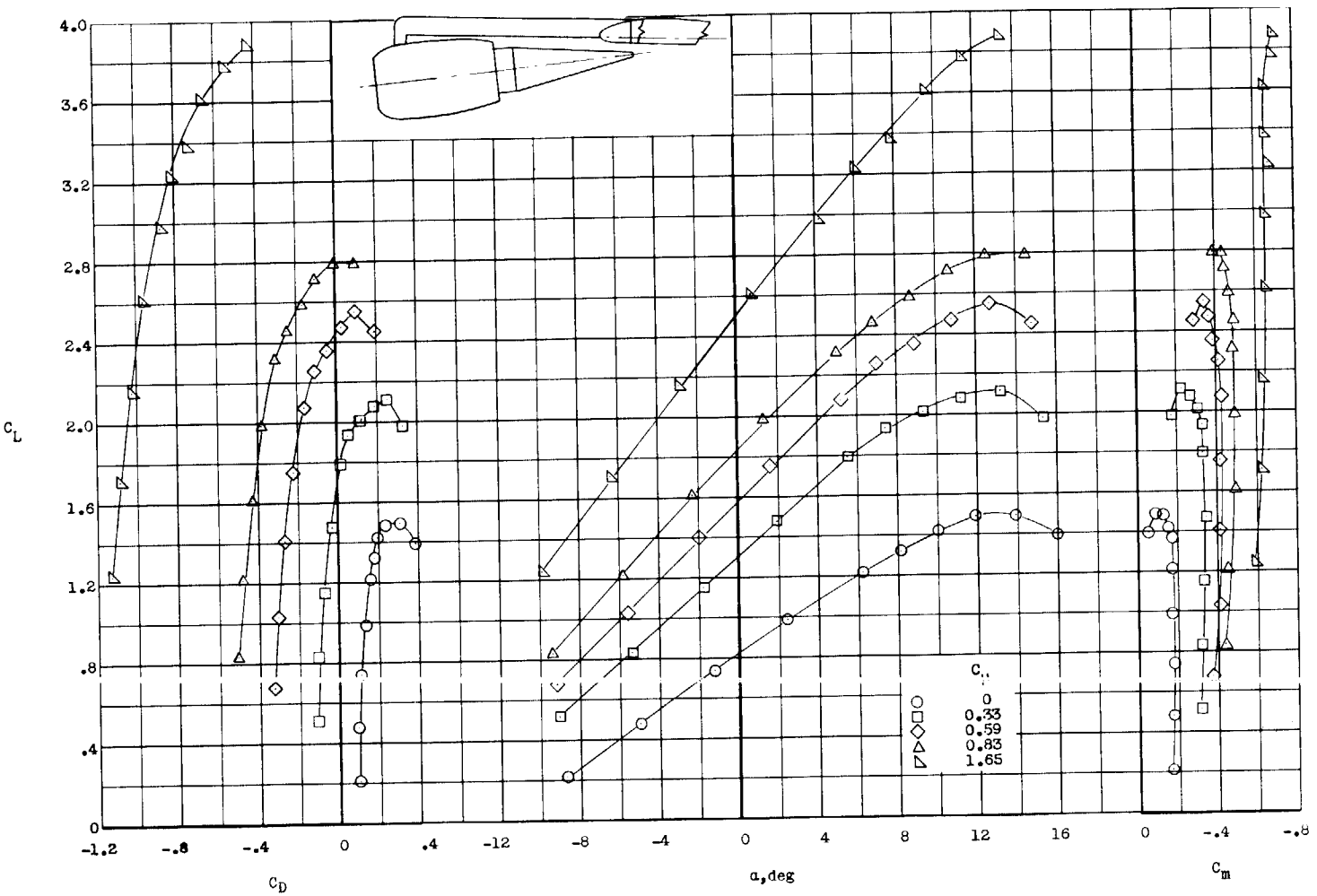

(a) $\delta_f = 30^o$.

Figure 10.- Aerodynamic characteristics of the model with half-span flaps deflected.

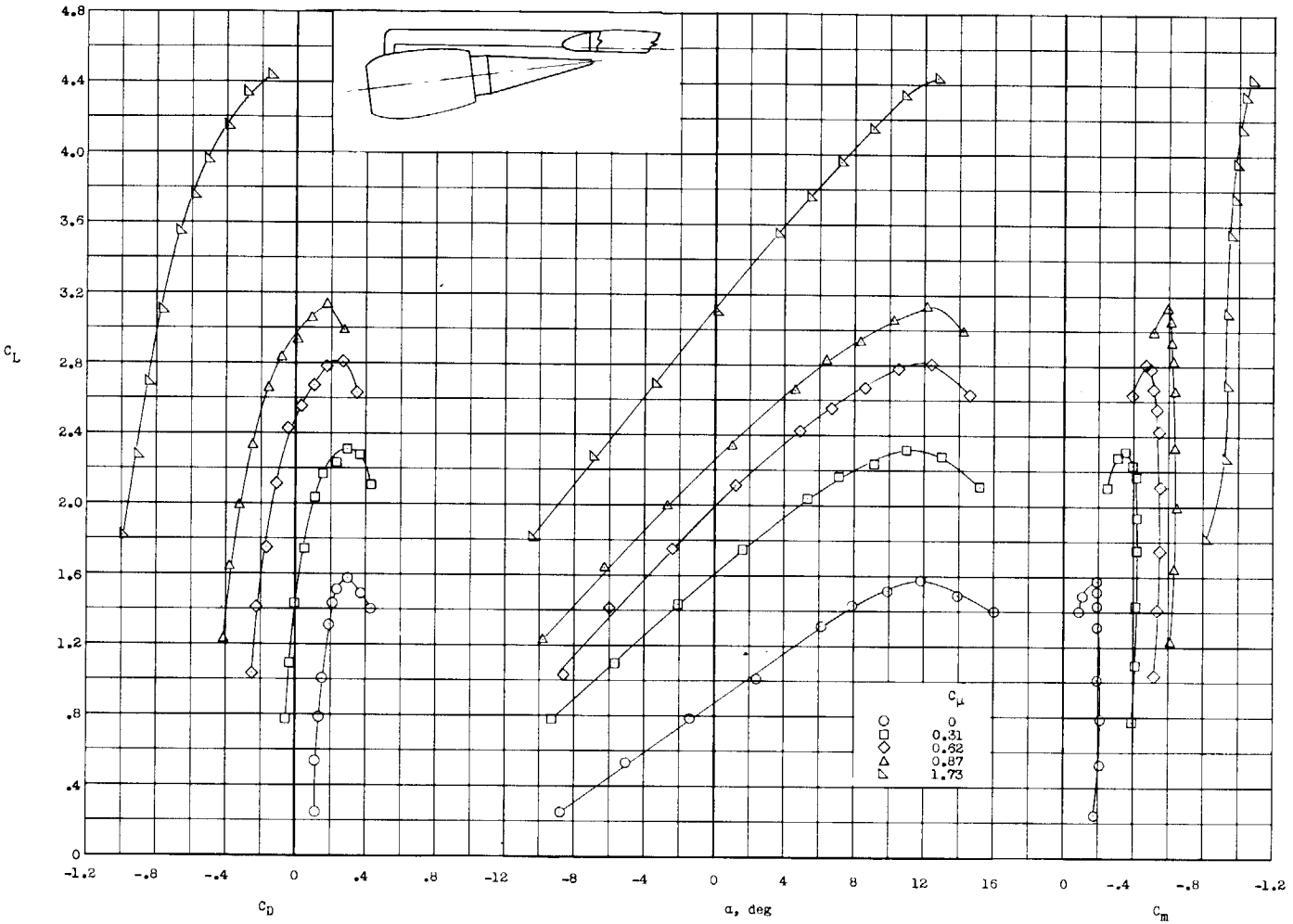

(b) $\delta_f = 40^\circ$.

Figure 10.- Continued.

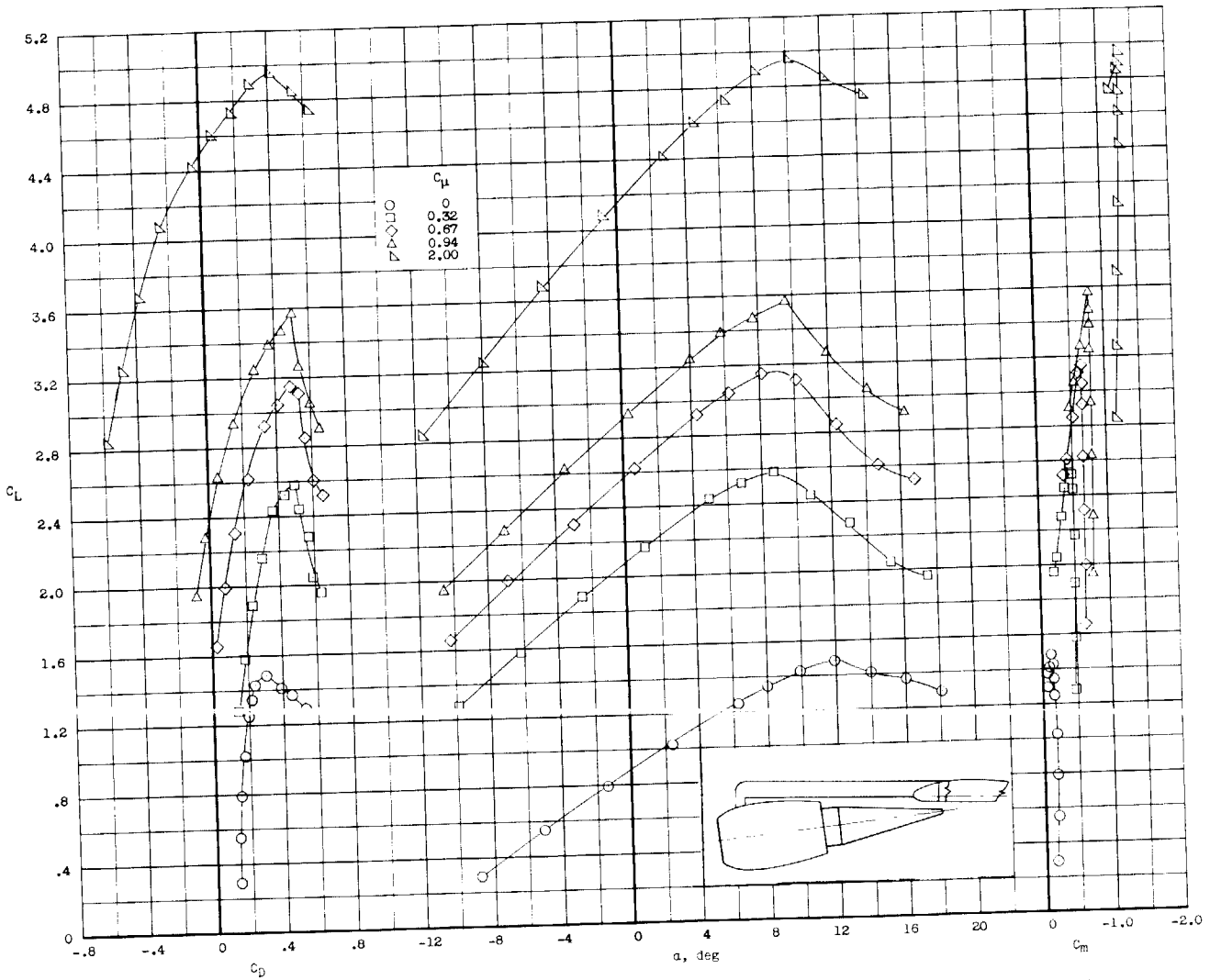

(c) $\delta_f = 60^\circ$.

Figure 10.- Concluded.

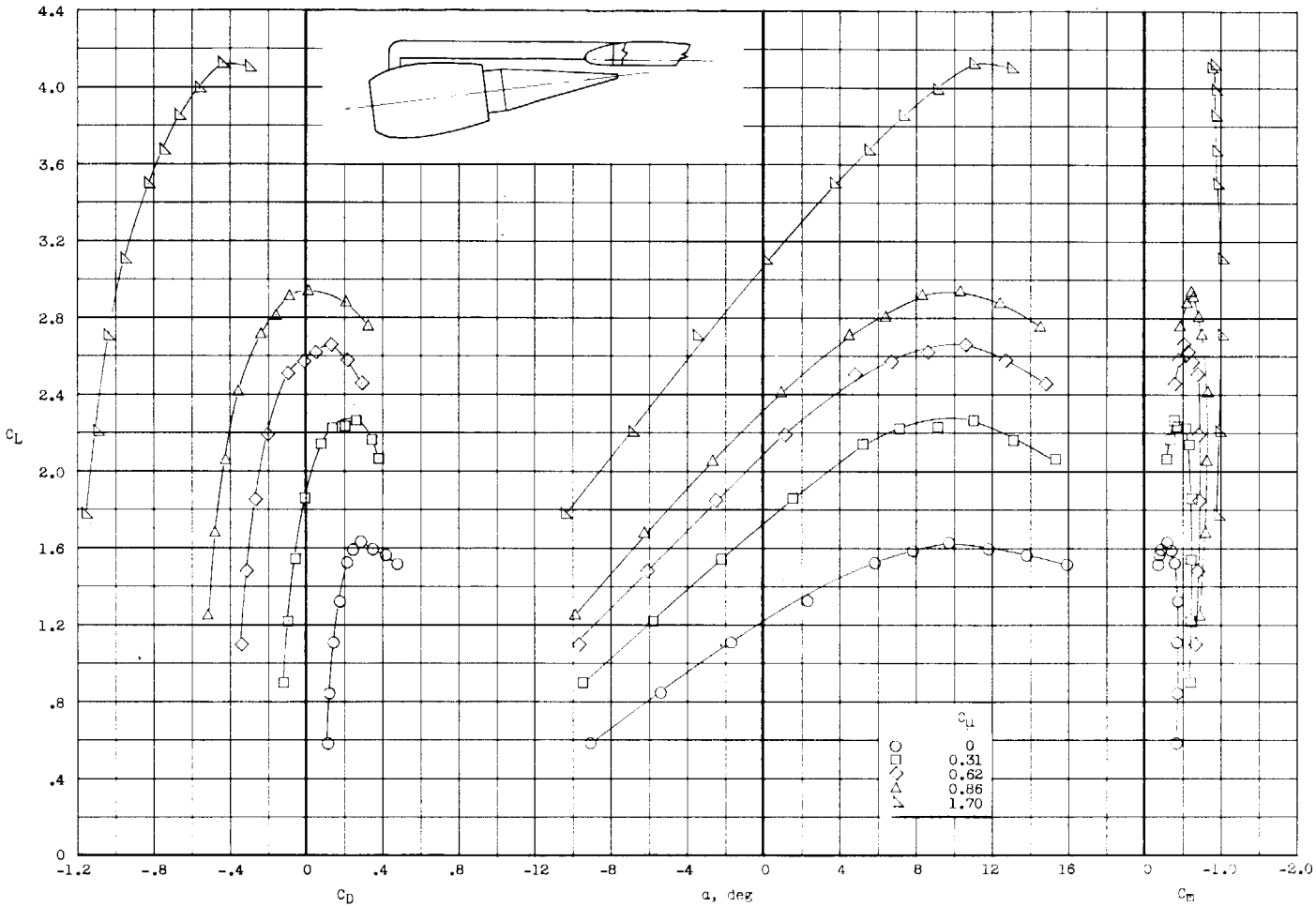

(a) $\delta_f = 30^\circ$.

Figure 11.- Aerodynamic characteristics of the model with full-span flaps deflected.

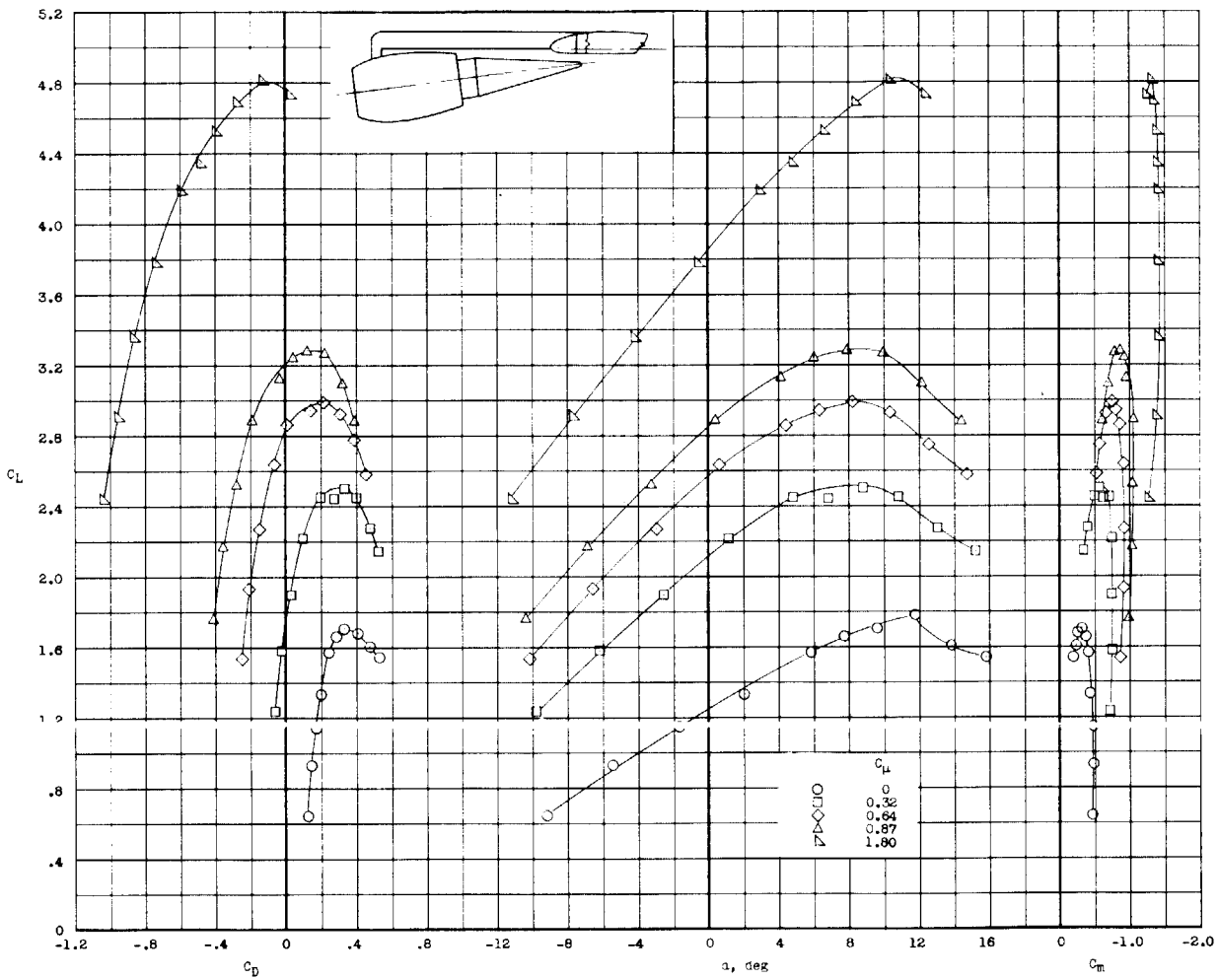

(b) $\delta_f = 40^o$.

Figure 11.- Continued.

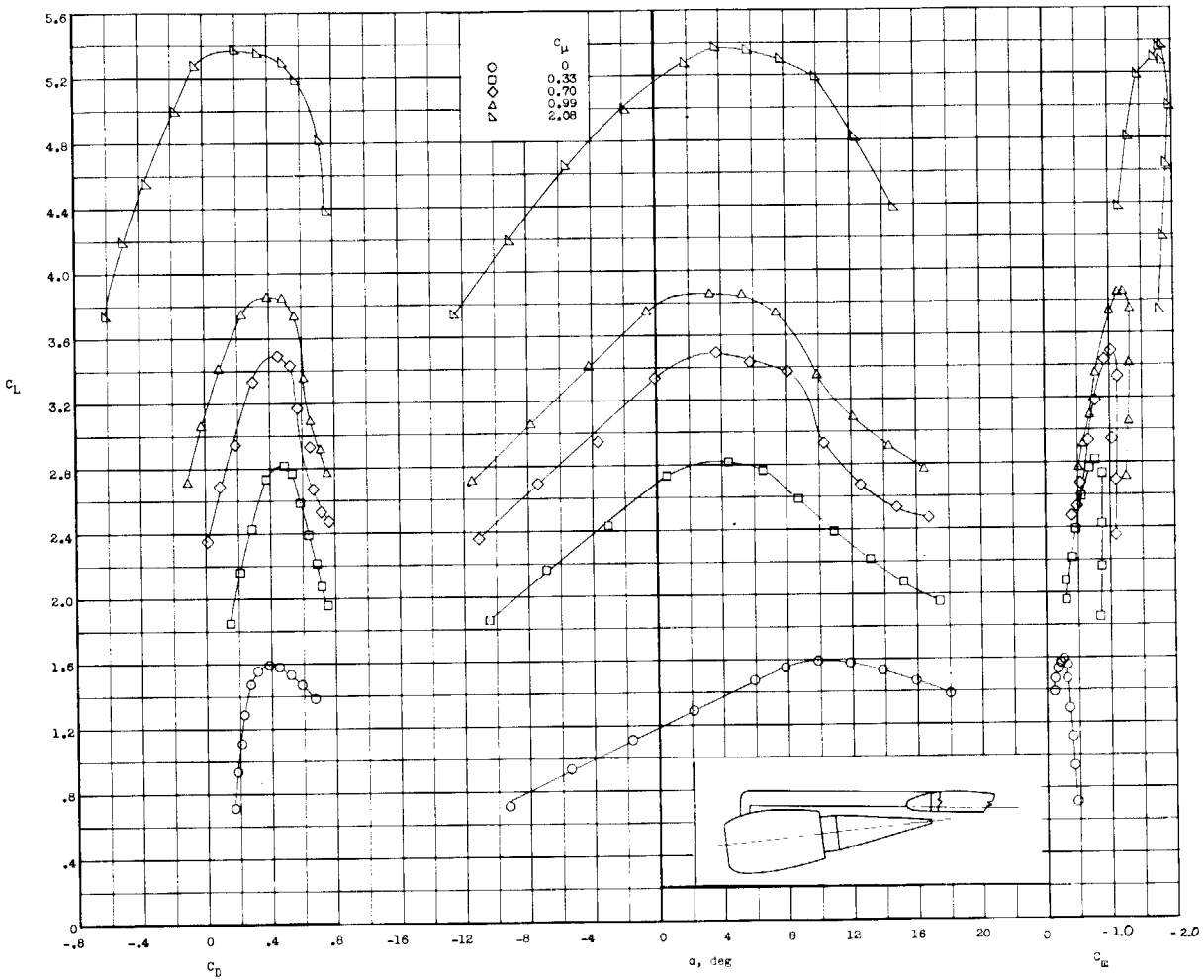

(c) $\delta_f = 60^\circ$.

Figure 11.- Concluded.

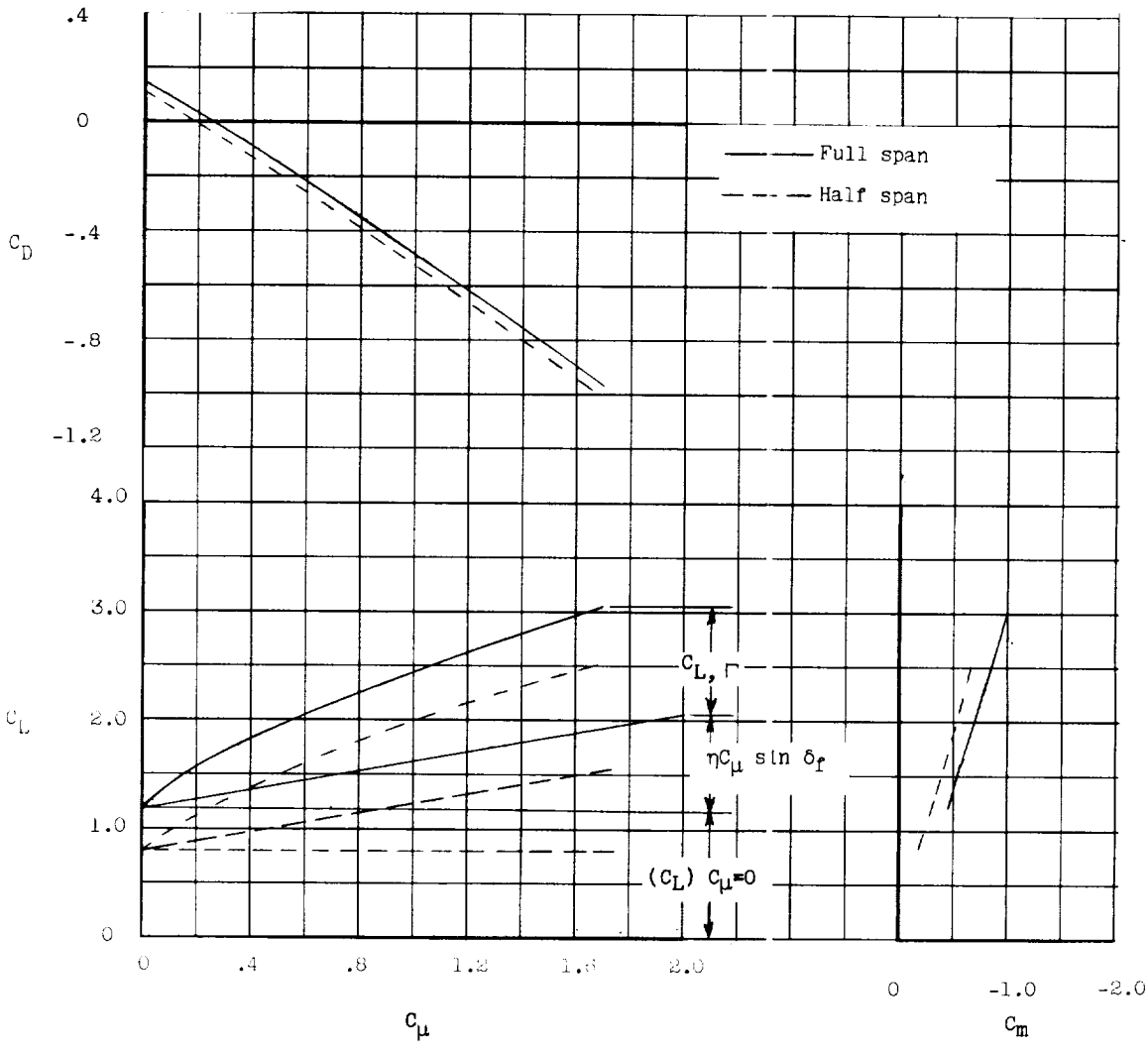

(a) $\delta_f = 30^\circ$.

Figure 12.- Variation of the aerodynamic characteristics with engine thrust coefficient for half- and full-span flaps. $\alpha = 0^\circ$.

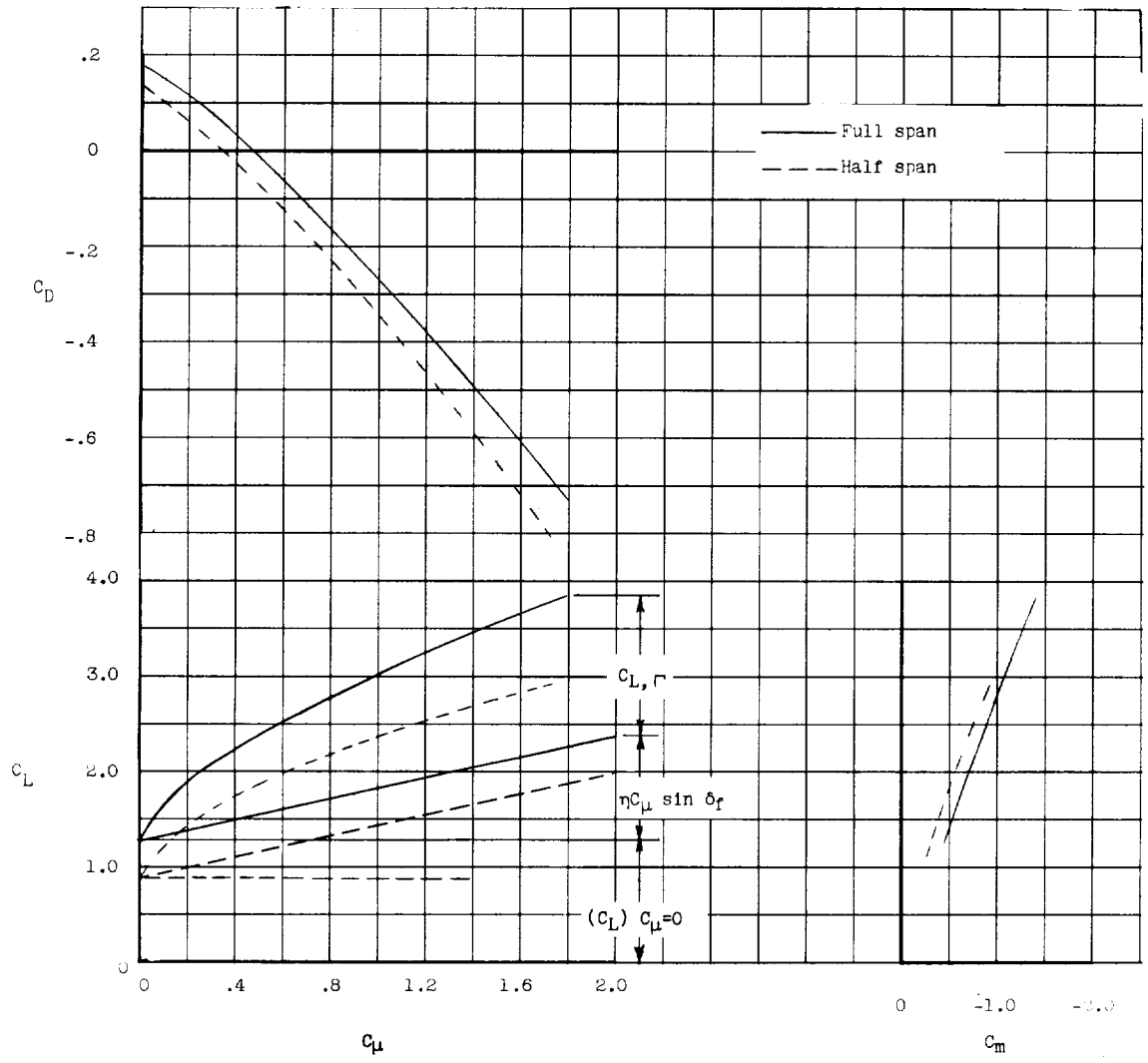

(b) $\delta_f = 40^\circ$.

Figure 12.- Continued.

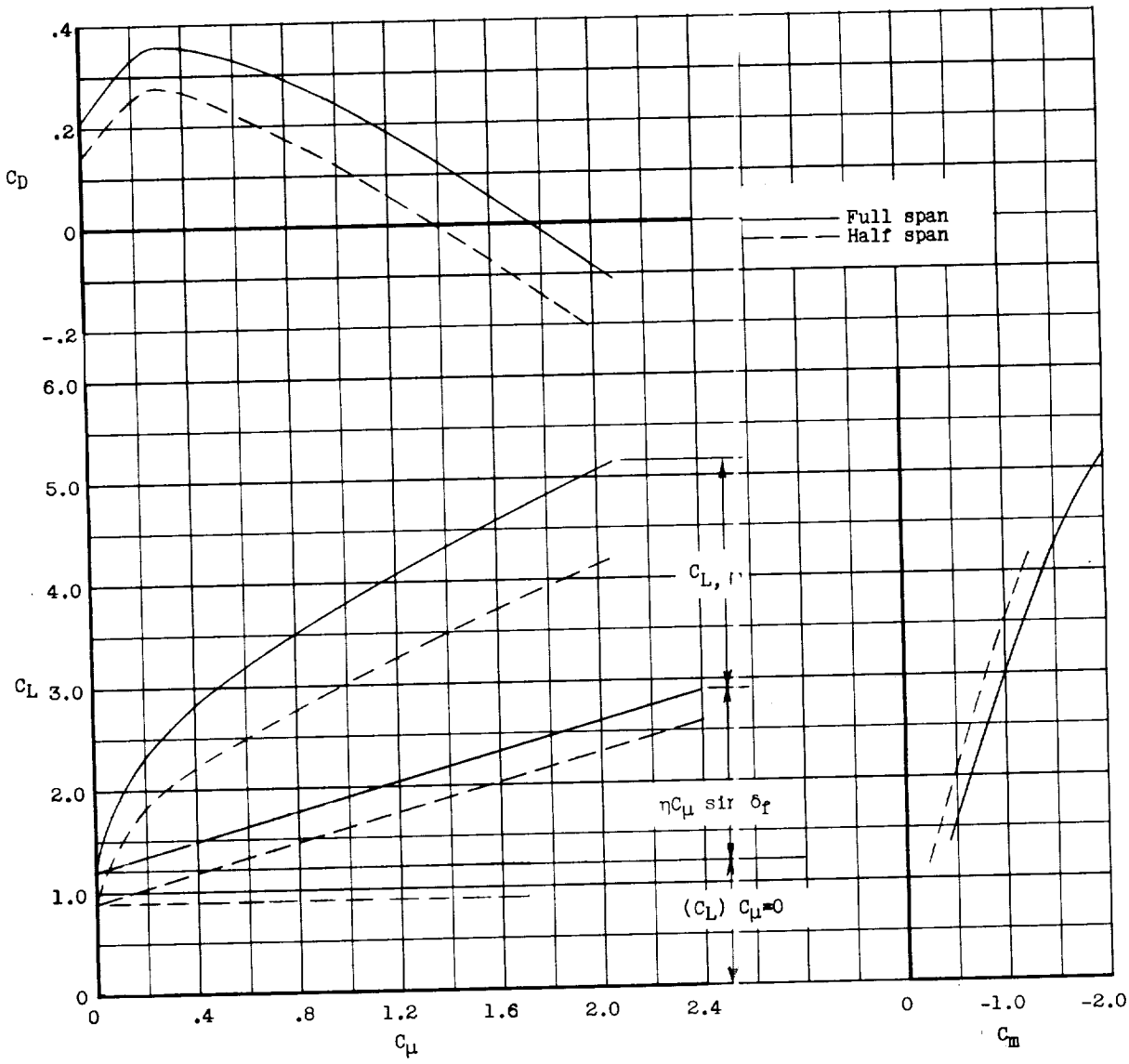

(c) $\delta_f = 60^\circ$.

Figure 12.- Concluded.

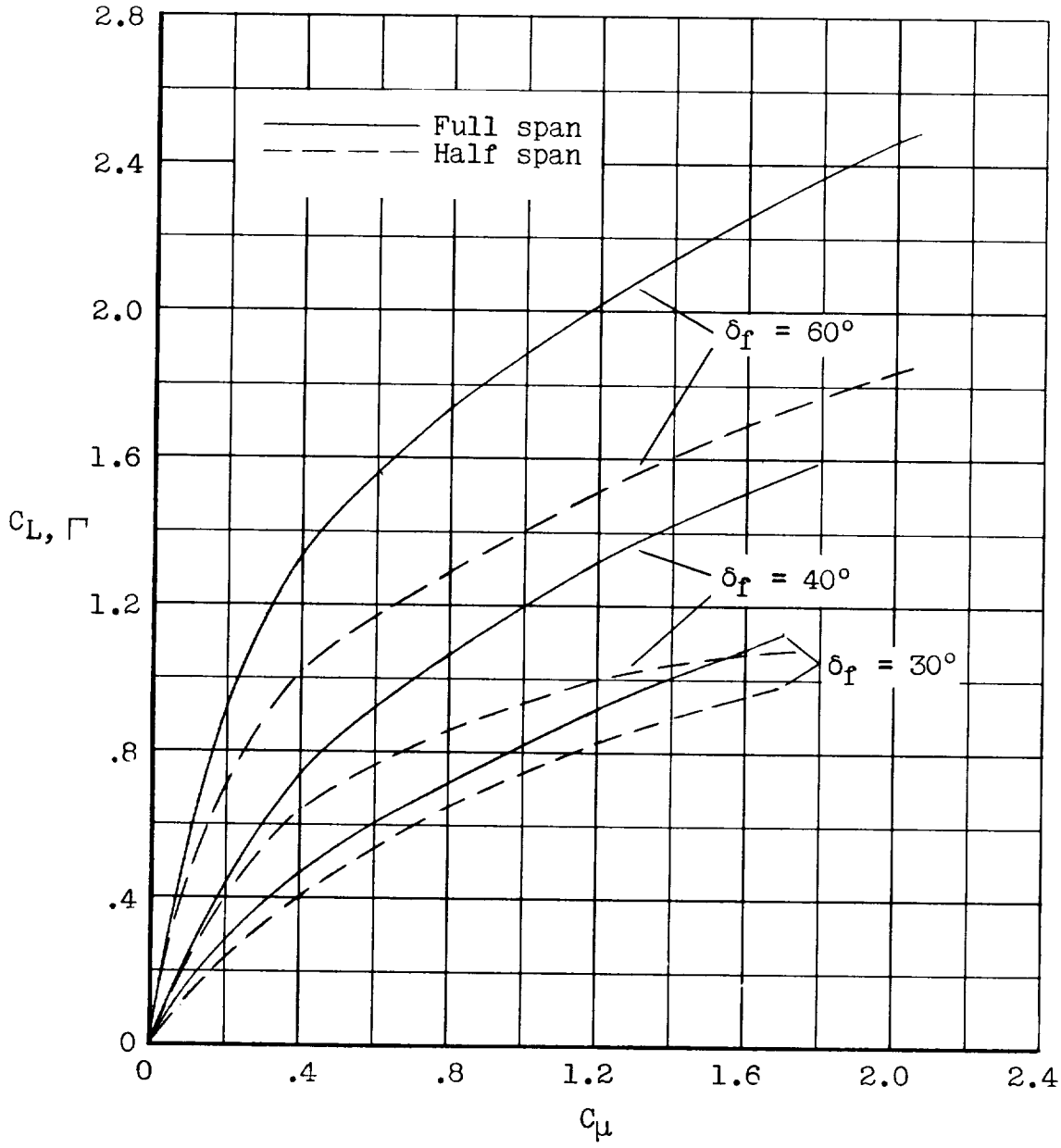

Figure 13.- Variation of circulation lift with momentum coefficient for half- and full-span flap configurations for several flap deflections.

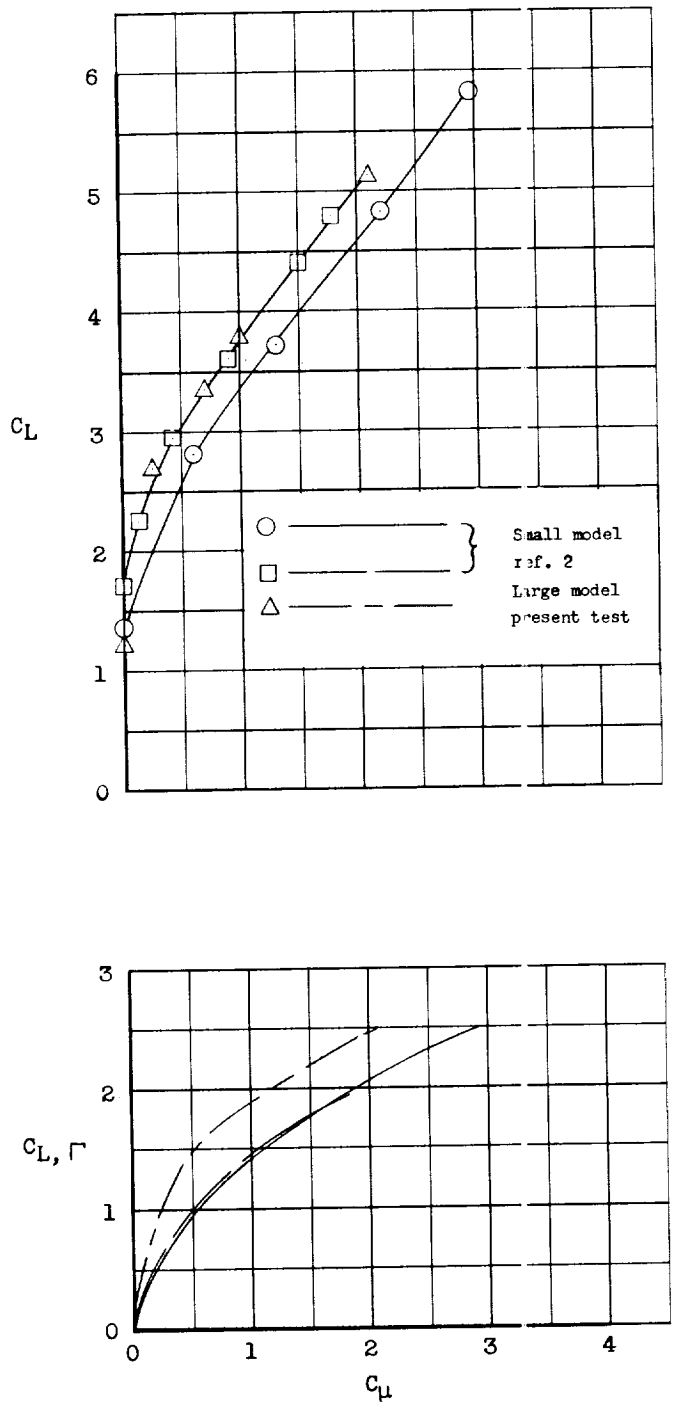

Figure 14.- Comparison of lift characteristics of two small models using cold air jets and the large-scale model using turbojet engines. $\alpha = 0^\circ$; $\delta_f = 60^\circ$.

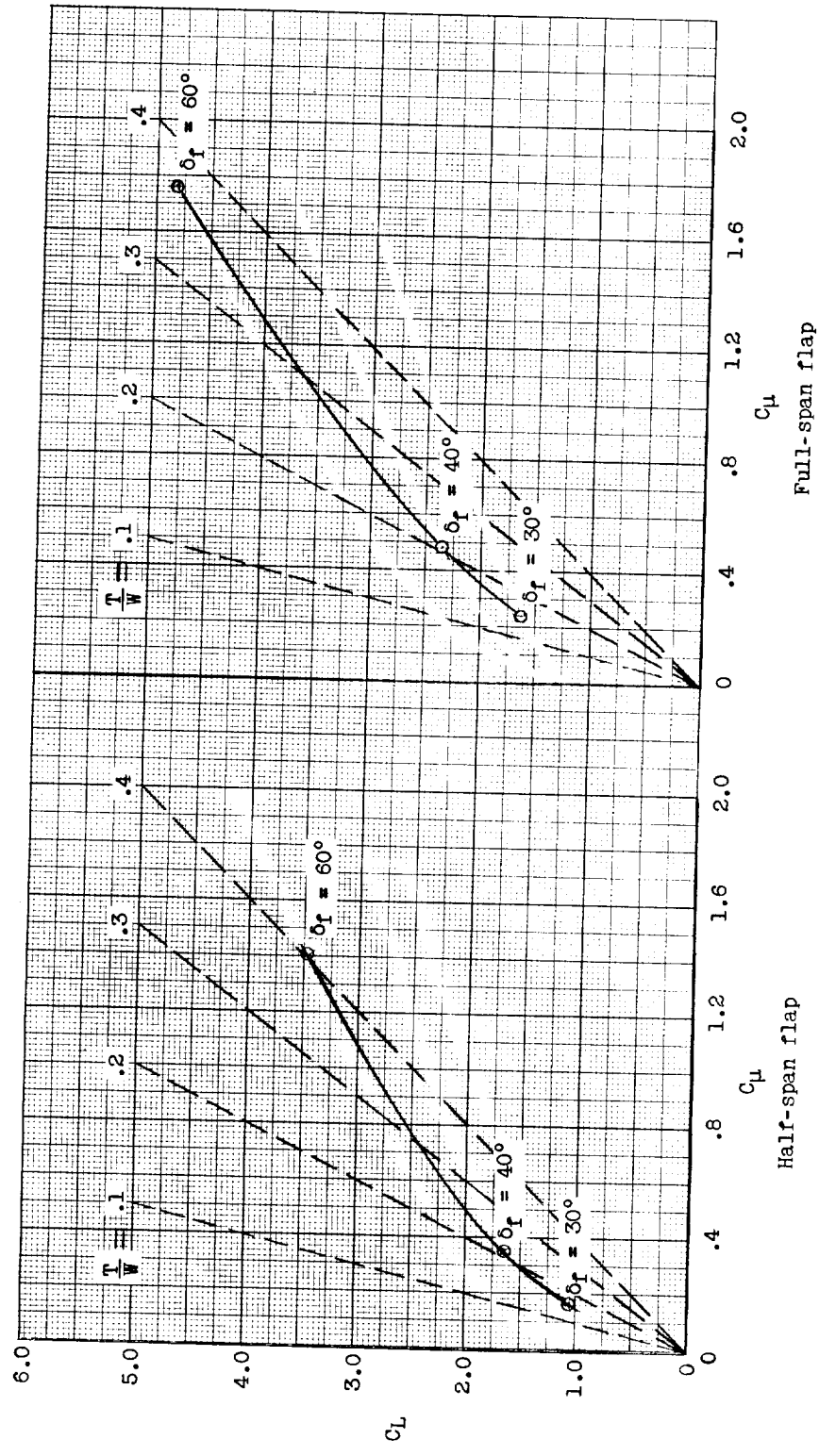

Figure 15.- Thrust-weight ratios at zero drag for several deflections of the half- and full-span flap with variations of C_L and C_μ.

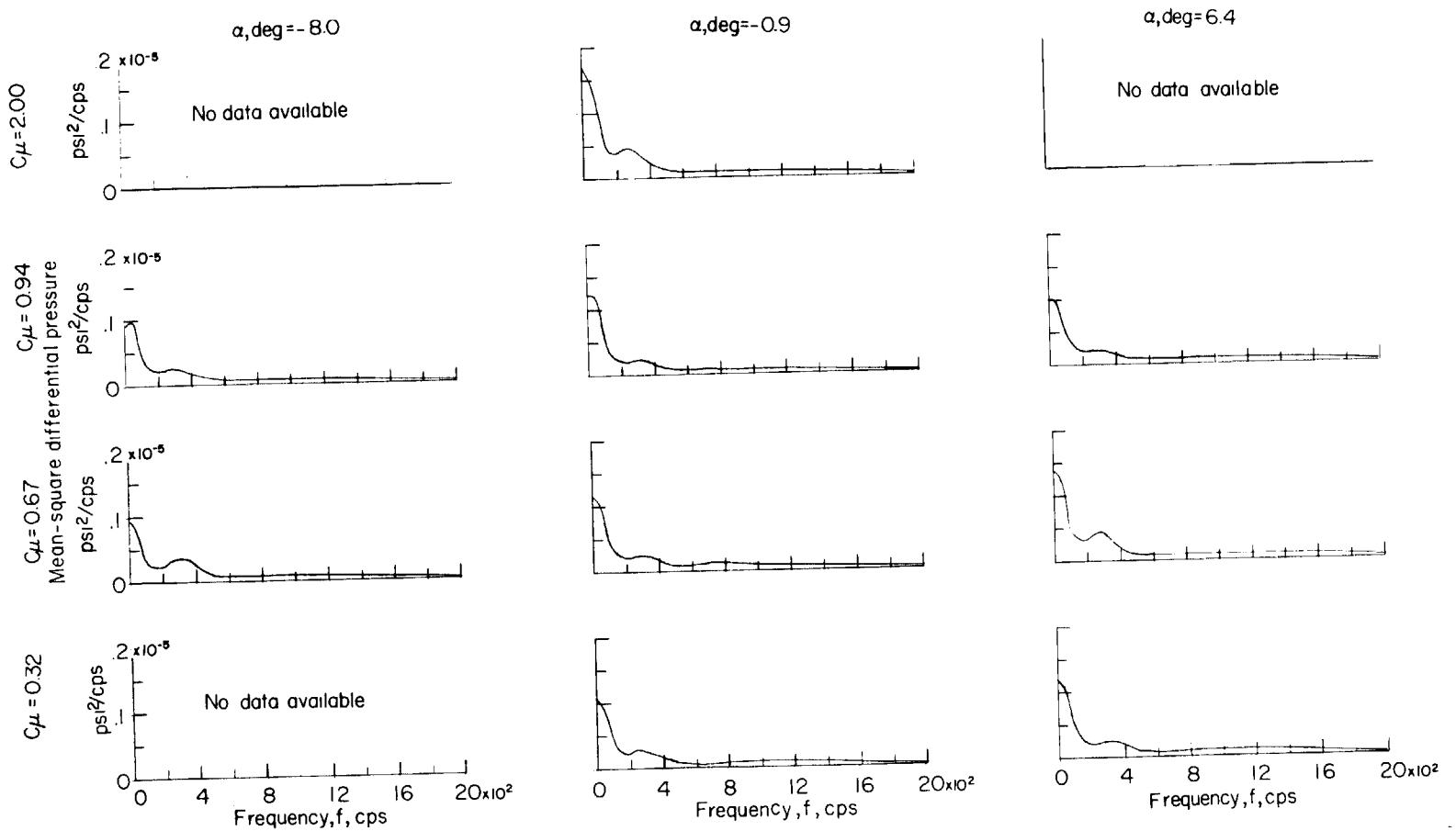

(a) Position A.

Figure 16.- Sound power-spectral-density analyses for several locations on the undersurface of the wing and flap.

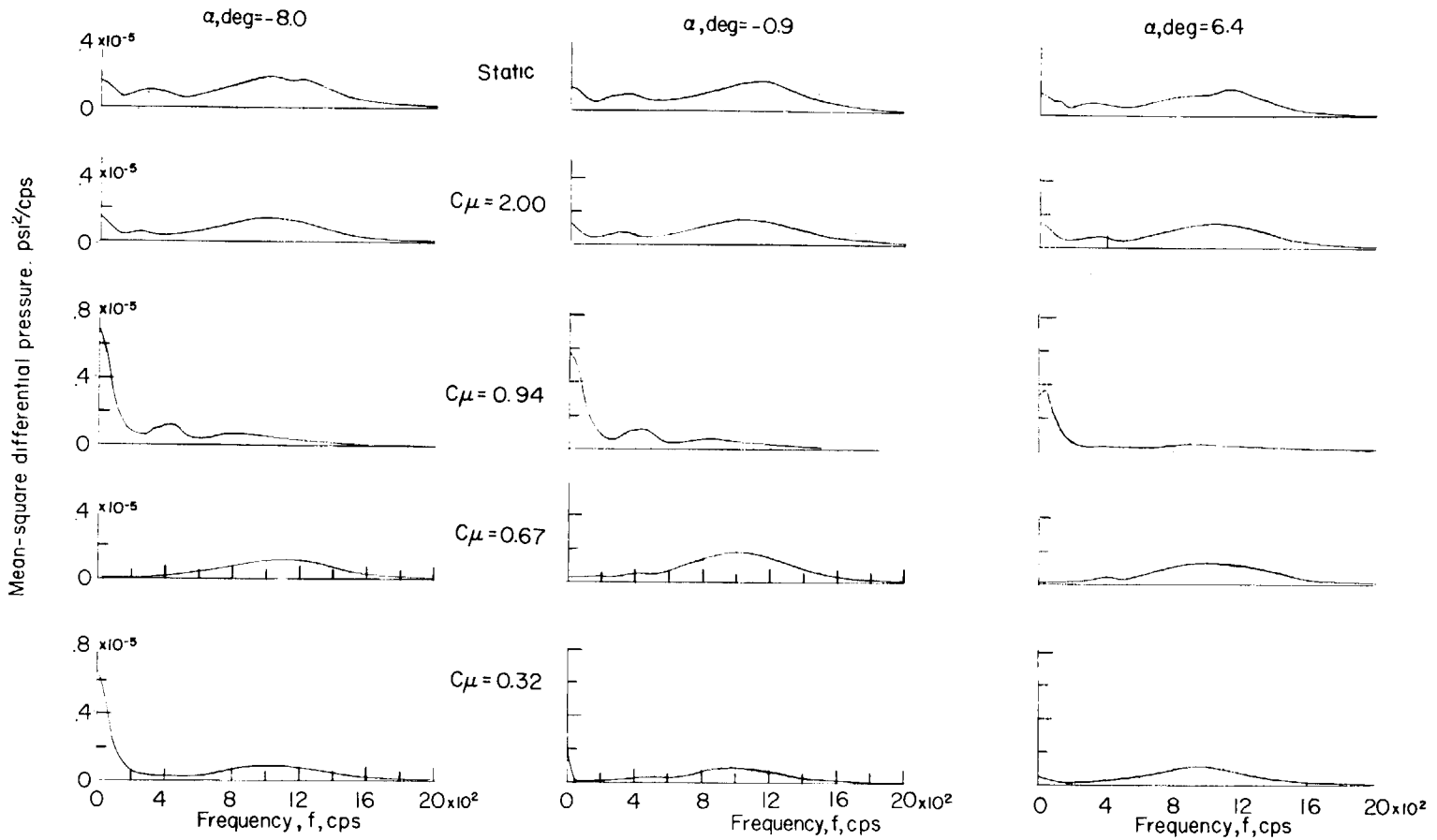

(b) Position B.

Figure 16.- Continued.

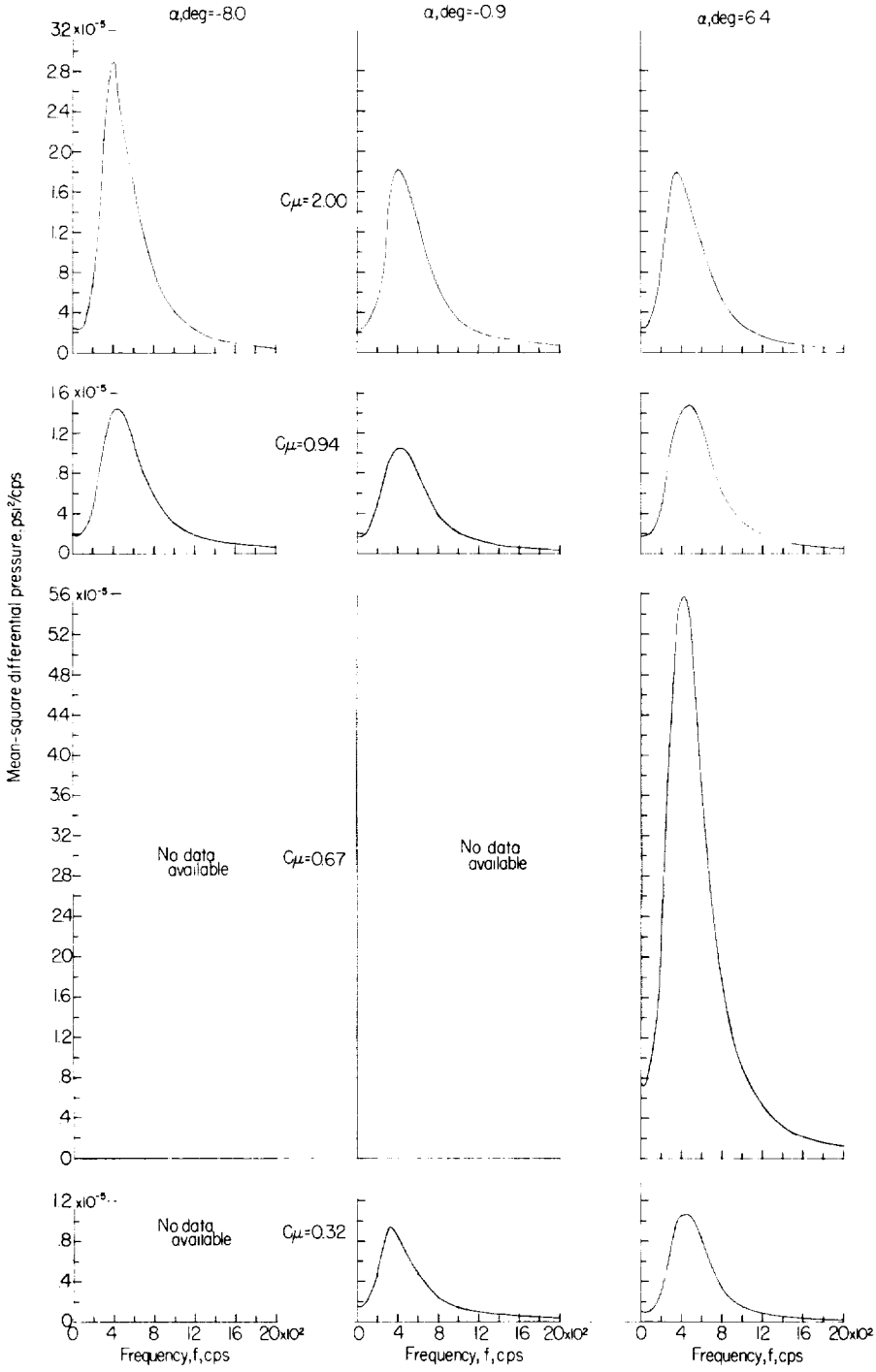

(c) Position C.

Figure 16.- Continued.

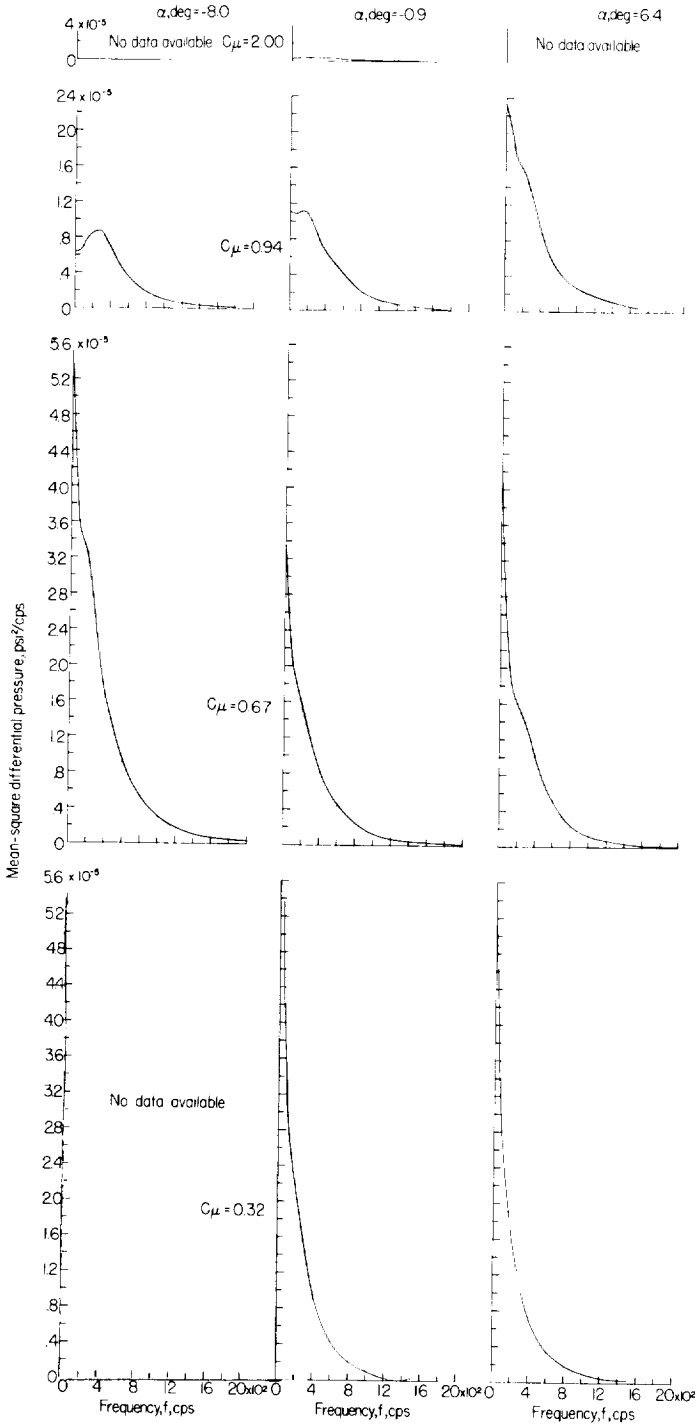

(d) Position D.

Figure 16.- Continued.

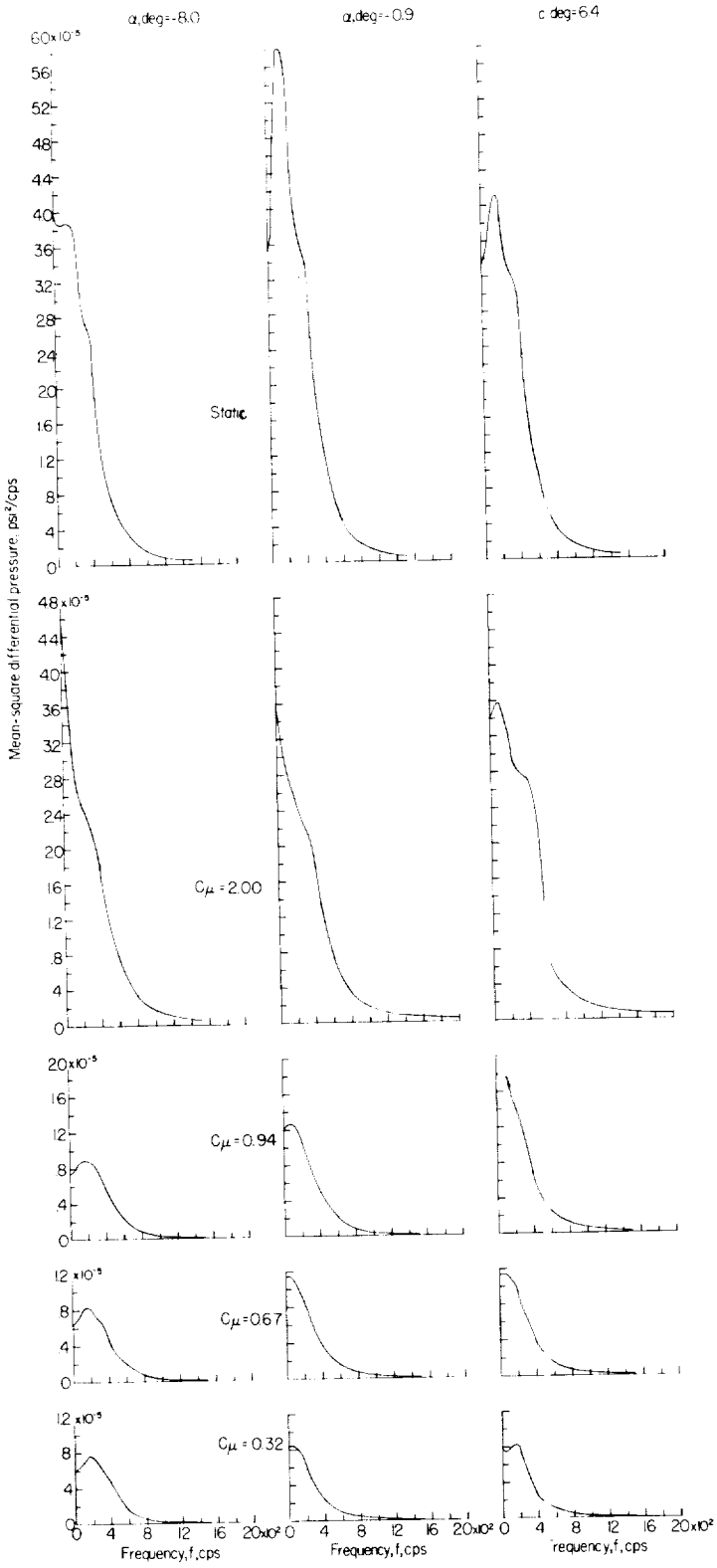

(e) Position E.

Figure 16.- Continued.

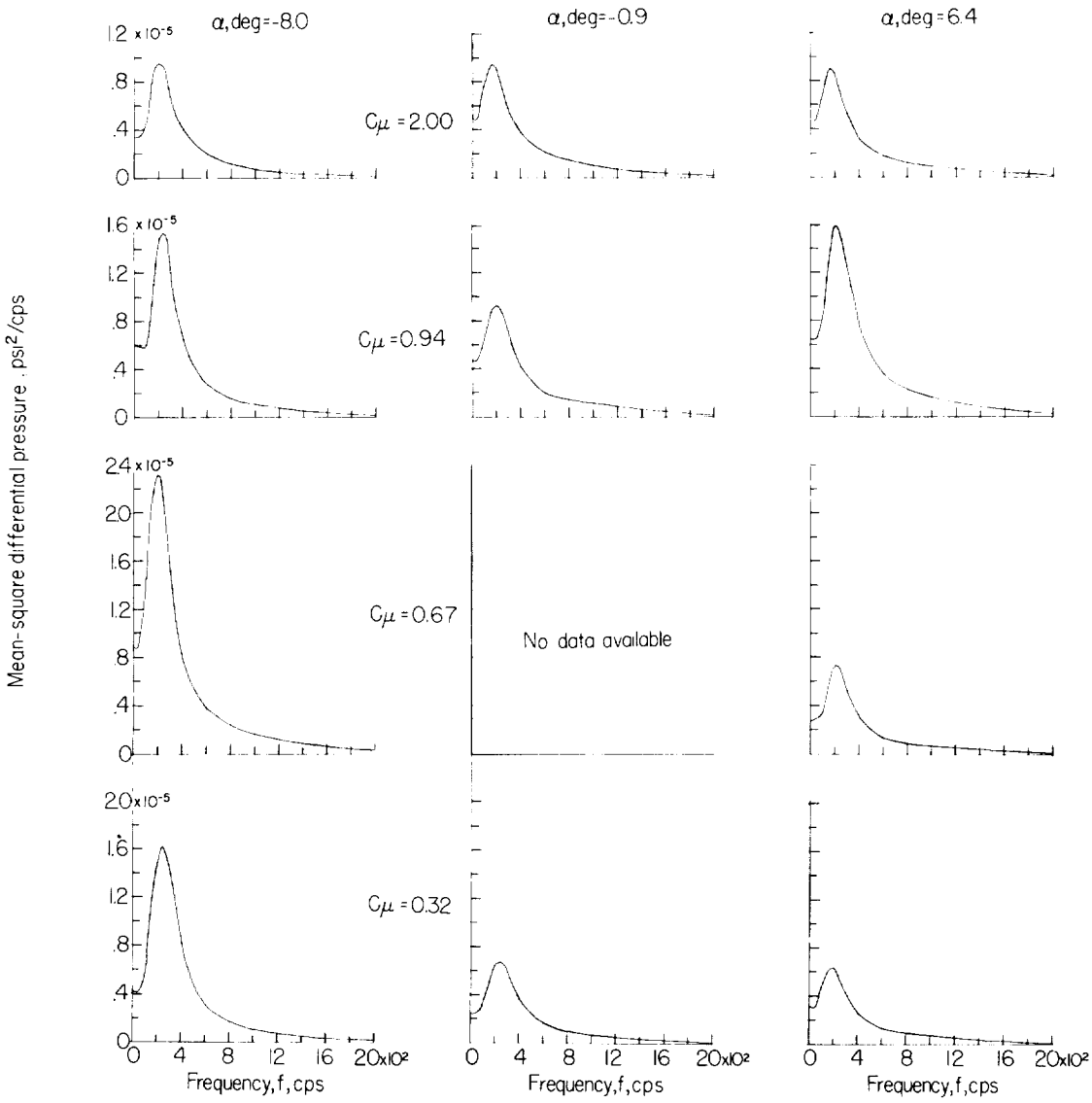

(f) Position G.

Figure 16.- Continued.

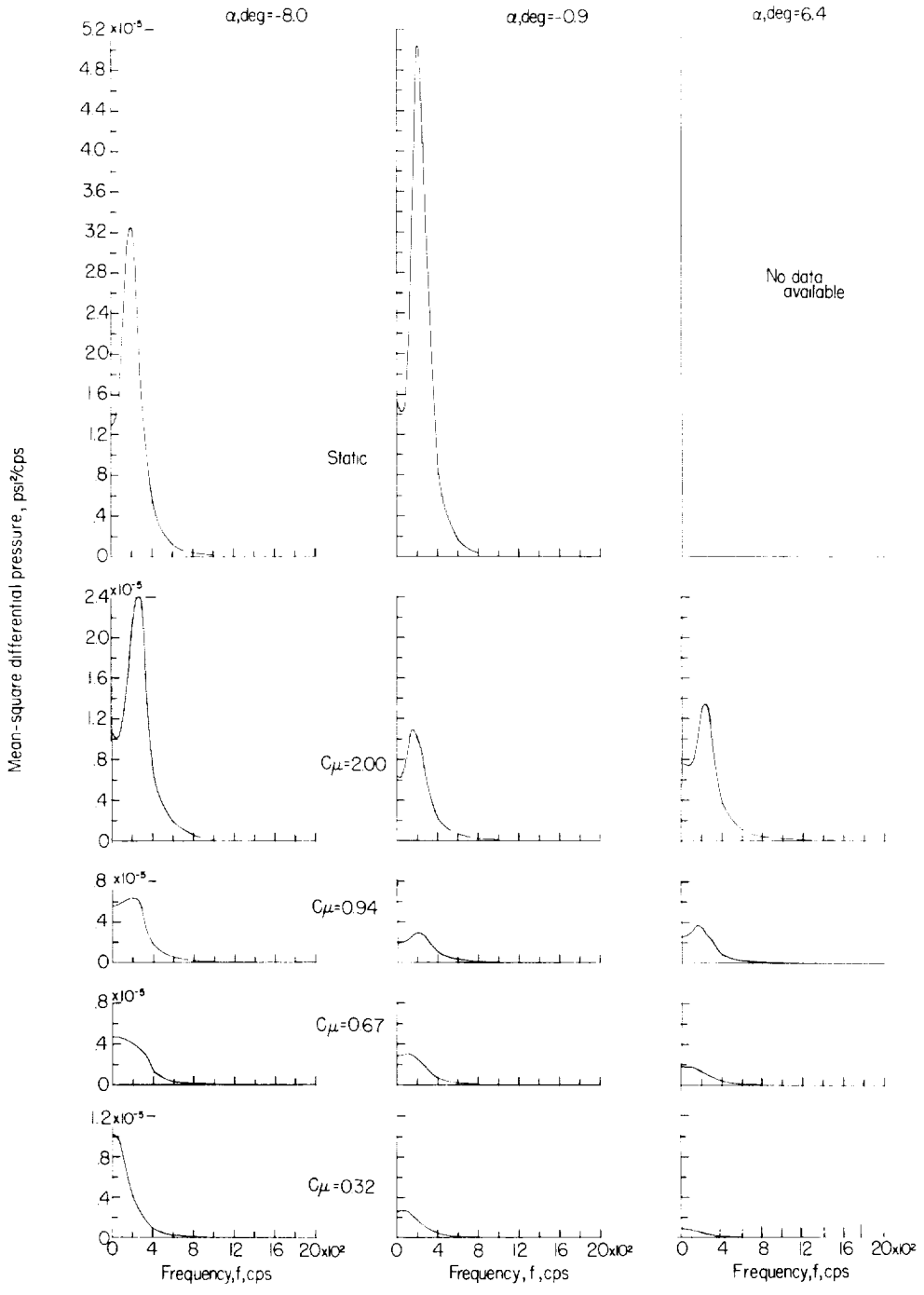

(g) Position H.

Figure 16.- Continued.

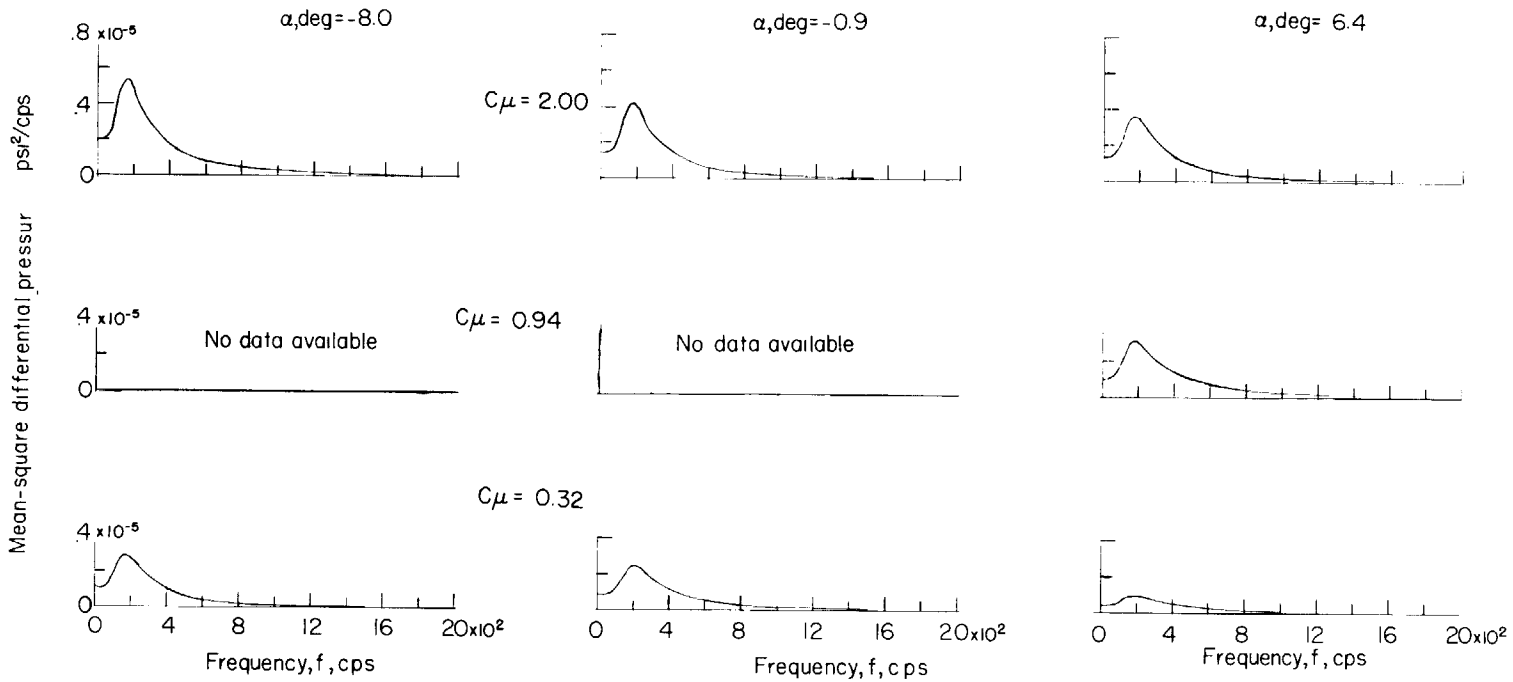

(h) Position I.

Figure 16.- Continued.

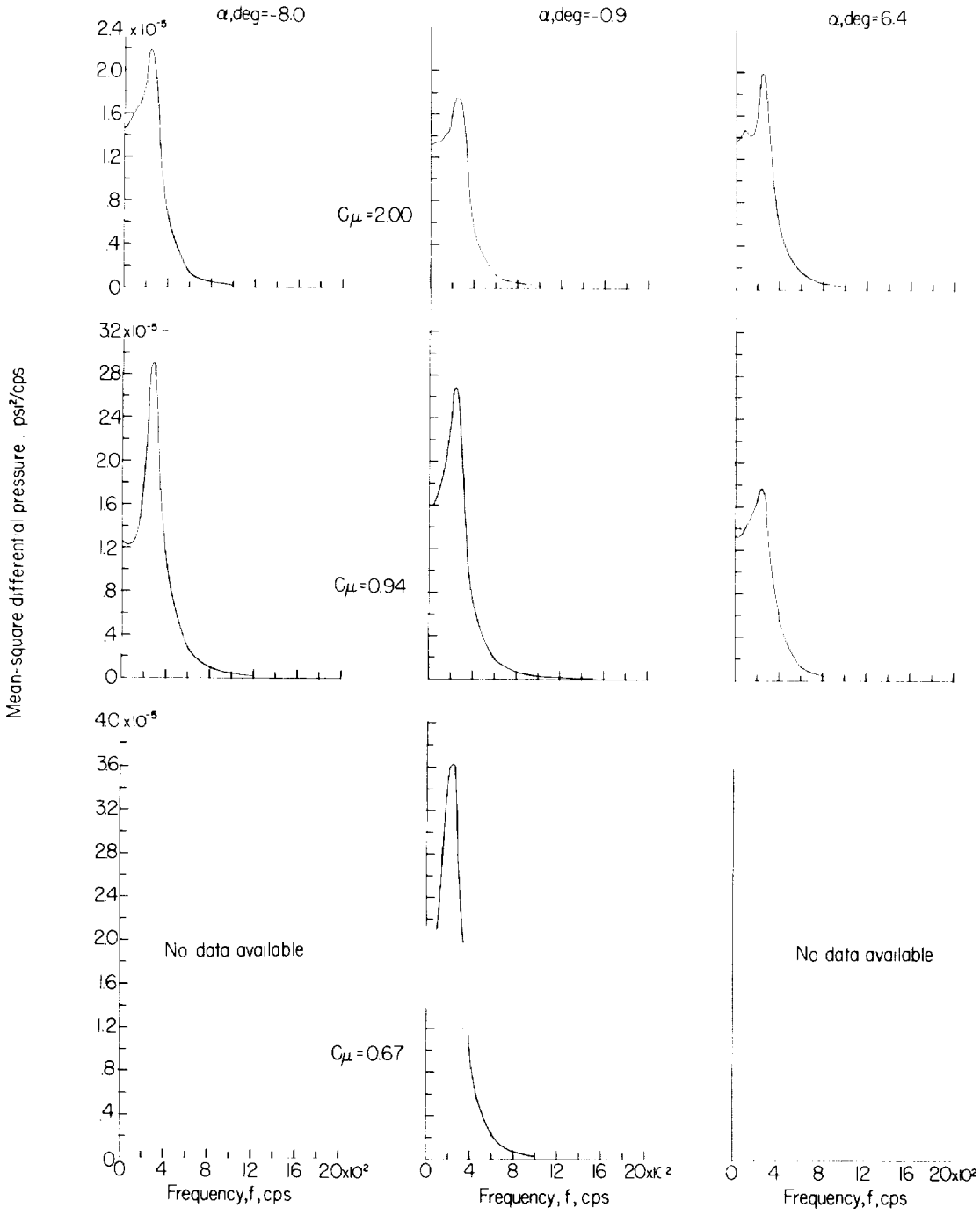

(i) Position J.

Figure 16.- Concluded.

L-1366